THE PENNSYLVANIA STATE UNIVERSITY
SCHREYER HONORS COLLEGE

DEPARTMENT OF MATERIALS SCIENCE AND ENGINEERING

CORRELATION OF PROCESSING VARIABLES WITH PROPERTIES OF TWO-DIMENSIONAL TUNGSTEN DISELENIDE FABRICATED VIA METAL ORGANIC CHEMICAL VAPOR DEPOSITION

LORRAINE HOSSAIN
SUMMER 2015

A thesis
submitted in partial fulfillment
of the requirements
for a baccalaureate degree
in Materials Science and Engineering
with honors in Materials Science and Engineering

Reviewed and approved* by the following:

Joshua A. Robinson
Assistant Professor of Materials Science and Engineering
Thesis Supervisor

Elizabeth Kupp
Senior Research Associate
Honors Adviser

* Signatures are on file in the Schreyer Honors College.

ABSTRACT

Novel two-dimensional materials like WSe_2 display optimal properties for faster and more efficient electronic and optical devices. More efficient electronic devices derived from the tunable band gap of these transition metal dichalcogenide materials will see improvements in the National Academy of Engineering's (NAE) Grand Challenges of health informatics and virtual reality.

For the research contained in this thesis, a series of experiments was conducted, varying the substrate material, the pressure, temperature, duration, and gas flow ratios of the system during growth, and the cleaning process to prepare each substrate. The WSe_2 films are synthesized onto the various substrates via metal organic chemical vapor deposition, in which a precursor vapor is passed over the substrate with a carrier gas and forms the film from the heat and set pressure. The quality of the resulting WSe_2 film was analyzed via Raman spectroscopy, atomic force microscopy, photoluminescence, and field emission scanning electron microscopy. The analysis demonstrated that increasing the pressure of the chamber from 600 Torr to 800 Torr decreased the nucleation of triangles while increasing the domain size of triangles. Additionally, an increased growth temperature from 600 °C to 900 °C also decreased the nucleation density with an increase in domain size. The ratio of selenium to tungsten precursor also affected the synthesis, with lower selenium concentrations creating selenium deficiencies and tungsten-rich precipitants on the surface. With the sapphire substrate, films with about ten micron WSe_2 triangles were synthesized. The boron nitride substrates exhibited a different growth mechanism, screw dislocation, and produced smaller domain sizes than sapphire substrates grown under the same conditions.

TABLE OF CONTENTS

LIST OF FIGURES iv

LIST OF TABLES vi

LIST OF EQUATIONS vii

ACKNOWLEDGEMENTS viii

CHAPTER 1 BACKGROUND 1

1.1 Introduction 1
1.2 Synthesis of Tungsten Diselenide 2
1.2.1 Selenization of WO_3 (Oxygen Replacement) 2
1.2.2 Chemical Vapor Transport 4
1.2.3 Powder Vaporization 5
1.2.4 Chemical Vapor Deposition 6
1.2.5 Metal Organic Chemical Vapor Deposition 10
1.2.5.1 Tungsten Precursors 13
1.2.5.2 Selenium Precursors 15
1.3 Substrates for WSe_2 Growth 16
1.3.1 Sapphire 17
1.3.2 Graphene 18
1.3.3 Boron Nitride 19
1.4 Motivation 20
1.4.1 Engineering Considerations 21

CHAPTER 2 PROCEDURE 23

2.1 Substrate Cleaning Procedure 23
2.2 Deposition System Preparation and Safety 24
2.3 WSe_2 Synthesis via Metal Organic Chemical Vapor Deposition 27
2.4 Data Analysis 28
2.4.1 Raman Spectroscopy 29
2.4.2 Photoluminescence 31
2.4.3 Atomic Force Microscopy 32
2.4.4 Field Emission Scanning Electron Microscopy 33

CHAPTER 3 RESULTS AND DISCUSSION 33

3.1 Preparation Study 33
3.2 Tungsten Diselenide on Sapphire 35
3.3 Tungsten Diselenide on Epitaxial Graphene 41
3.4 Tungsten Diselenide on Amorphous Boron Nitride 45

CHAPTER 4 CONCLUSION........51

BIBLIOGRAPHY........53

LIST OF FIGURES

Figure 1. Experimental setup for chemical vapor transport[5] 5

Figure 2. Experimental setup for powder vaporization 6

Figure 3. Growth mechanisms for chemical vapor deposition describe the interactions between reactant gasses and the substrate.[8] 7

Figure 4. Chemical Vapor Deposition Setup[9] 8

Figure 5. Schematic of a bubbler system[12] 10

Figure 6. The MOCVD chamber is set up to heat the substrate through induction heating on a susceptor. a) Image of MOCVD Chamber with heated susceptor; 12

Figure 7. Temperature profile of WSe_2 deposition via MOCVD 28

Figure 8. Typical Raman Spectra for WSe_2 on Sapphire Substrate 30

Figure 9. Experimental Setup of Photoluminescence Measurement[23] 31

Figure 10. Photoluminescence signals from monolayer, bilayer, and bulk WSe_2[2] 32

Figure 11. AFM images of sapphire substrates cleaned via standard wet cleaning or addition oxygen or argon etching demonstrate no increase of domain size (300 nm) compared to standard process. 34

Figure 12. Profile of Tungsten Hexacarbonyl Exposure Time Study 35

Figure 13. Varying exposure time of the tungsten source affected the nucleation and particle density of the WSe_2. 36

Figure 14. Temperature Profile for WSe_2/Sapphire at Varying Temperatures 37

Figure 15. AFM images of samples grown at 750 ^oC, 800 ^oC, 825 ^oC, and 850 ^oC demonstrate increased domain size from 650nm to 1 micron 37

Figure 16. Raman spectra for WSe_2/Sapphire samples grown at different temperatures 38

Figure 17. AFM images of WSe_2/Sapphire with varying Se:W ratios. a) Se:W = 170; b) Se:W = 400; c) Se:W = 800; d) Se:W = 14,000; e) Se:W = 20,000; f) Se:W = 100,000 39

Figure 18. AFM of WSe_2/Sapphire synthesized at different total hydrogen flow rates shows an increase in domain size as total flow increases. 40

Figure 19. AFM images of epitaxial graphene grown at a Se:W ratio of 170 with varying temperature shows an increase in domain size as temperature increases. 41

Figure 20. AFM images of WSe_2/sapphire samples grown at various growth temperatures show poor nucleation compared to the graphene in Figure 19. 42

Figure 21. FESEM of WSe_2/EG samples demonstrate increased nucleation as Se:W increases. a) Se:W= 170 @ 825 ºC; b) Se:W=500 @ 825 ºC; c) Se:W=609 @ 800 ºC; d) Se:W=700 @ 825 ºC 43

Figure 22. AFM images of WSe_2/EG compared to WSe_2/Sapphire under same conditions at higher Se:W ratio. a) WSe_2/EG; b) WSe_2/Sapphire 44

Figure 23. AFM of WSe_2/BN synthesized at different pressures show that increasing the pressure increases domain size and reduces particle density. 45

Figure 24. AFM of WSe_2/BN at different Se:W ratios demonstrate an increased domain size with increased Se:W. a) Se:W=130; b) Se:W=590 46

Figure 25. AFM images of WSe_2 on both a sapphire and amorphous boron nitride substrates synthesized under the same conditions. a) WSe_2/Sapphire with total H_2 flow = 100 sccm; b) WSe_2/a-BN with total H_2 flow = 100 sccm; c) WSe_2/Sapphire with total H_2 flow = 250 sccm; d) WSe_2/a-BN with total H_2 flow = 250 sccm..47

Figure 26. AFM images of WSe_2 on a-BN synthesized with different total flows of hydrogen in the MOCVD system. a) Total flow = 100 sccm H_2; b) Total flow = 250 sccm H_2..........48

Figure 27. AFM of a-BN before and after an oxygen etch shows reduced roughness after etching. a) Pre-etched BN; b) Post-etched BN 49

Figure 28. AFM of WSe_2 on etched a-BN shows high particle density of 25 particles/square micron and small domain size of 200nm. a-d) different areas on the sample 50

LIST OF TABLES

Table 1. Common Peaks in WSe_2 Raman Spectra 29

Table 2. Roughness values for pre-etched BN compared to post-etched BN 49

LIST OF EQUATIONS

Equation 1. Selenization reaction to form WSe_2 from WO_3 3

Equation 2. Partial Pressure of Tungsten Hexacarbonyl Precursor 14

Equation 3. Concentration of vaporized Tungsten Hexacarbonyl Precursor 15

Equation 4. Partial Pressure of Dimethyl Selenium Precursor.. 16

Equation 5. Concentration of Vaporized Dimethyl Selenium Precursor 16

ACKNOWLEDGEMENTS

I would like to thank Dr. Joshua Robinson for providing me with the opportunity to conduct this research and guiding me through the process. Many thanks go to Dr. Sarah Eichfeld for her mentorship throughout my research: training me on equipment and providing extensive advice on data analysis and thesis writing. Additionally, Dr. Kupp, Dr. Kimel, and Ms. Cindy Lake provided valuable advising. I would also like to acknowledge Dr. Jarod Gagnon and Yu-Chuan Lin for their advice and encouragement during data analysis. Alek Piasecki, Benjamin Kupp, and Lauren Weiss also contributed with this research. This research was supported by the Center for Low Energy Systems Technology (LEAST), which is a center under the STARnet phase of the Focus Center Research Program (FCRP), a Semiconductor Research Corporation (SRC) group funded by MARCO and DARPA. Finally, I wish to thank my family and friends for their continued love and support.

CHAPTER 1

BACKGROUND

1.1 Introduction

Transition metal dichalcogenides (TMDs) have received increased attention since their electronic properties allow them to behave as both metals and wide-gap semiconductors. This opens up possibilities for their application in chemical and biological sensors, thermal management, optoelectronics, and ultracapacitors[1]. TMDs consist of a metal atom (i.e. Mo, W) bonded with two elements in the chalcogen column of the Periodic Table of Elements (i.e. Se, S, Te) in the form MX_2[1]. The structure of these materials are either trigonal prismatic or octahedral. Similar to graphene, TMDs can be synthesized into two dimensional materials, meaning the thin film can have a thickness of only one atom. In the plane of this monolayer, strong covalent bonds hold the metal and chalcogen together, while weak van der Waals forces dominate between planes of film layers[1]. Atomically thin WSe_2 contains strong covalent bonding between tungsten and selenium atoms, with weaker van der Waals bonding in the c-plane perpendicular to the plane of the film. This reduces the dangling bonds at the surface of the film. Nucleation of tungsten diselenide thin films form in the shape of triangles, and several growth mechanisms are observed with the addition of secondary nucleation sites, such as screw dislocations and layer-by-layer growth beginning from the center of a preexisting triangle or along the step edge of the triangle[1]. Tungsten diselenide provides unique electronic and optical properties with its intrinsic bandgap of about 1.2 eV[2]. This bandgap falls into the optimal range for fast and efficient

electronic devices, plus the bandgap is intrinsically present, meaning no dopants are needed to alter the bandgap[1]. In this sense, tungsten diselenide holds an advantage over the intrinsically conductive graphene. Additionally, tungsten diselenide transitions from an indirect bandgap, in which momentum or added direction is needed to excite electrons into the conduction band, to a direct bandgap when the material goes from bulk multilayers to a single monolayer[1]. Monolayer tungsten diselenide has a bandgap of about 1.65 eV, and exhibits photoluminescence[2]. Applications for tungsten diselenide range from solar cells, supercapacitors, lithium ion batteries, to electro-catalysis due to its transport properties[1].

1.2 Synthesis of Tungsten Diselenide

Several methods of tungsten diselenide synthesis have been analyzed, including powder vaporization, selenization, chemical vapor transport, chemical vapor deposition, and metal organic chemical vapor deposition. These techniques are described in the following sections.

1.2.1 Selenization of WO_3 (Oxygen Replacement)

Selenization of a tungsten precursor like WO_3 is one technique that forms WSe_2 thin films. For selenization, a layer of tungsten trioxide (WO_3) is deposited via a method like thermal evaporation onto a sapphire substrate. Then the sample is exposed to a selenium source, and oxygen from the tungsten trioxide is replaced by the selenium. Selenization can occur via techniques like chemical vapor transport and chemical vapor deposition. The thermodynamic reaction, as selenium flows onto the WO_3 sample and replaces oxygen, can be illustrated with the following reaction:

Equation 1. Selenization reaction to form WSe_2 from WO_3

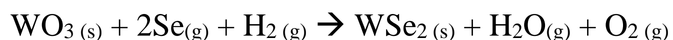

$$WO_{3\,(s)} + 2Se_{(g)} + H_{2\,(g)} \rightarrow WSe_{2\,(s)} + H_2O_{(g)} + O_{2\,(g)}$$

Galen and other colleagues utilized this technique in a reducing atmosphere and grew WSe_2 on quartz substrates[3]. For their study, Galen *et al.* also discovered that depositing an ultrathin layer of nickel or tin film, with a thickness between 3 to 10 nanometers, between the quartz substrate and the WO_3 film before selenization increases the crystallinity and texture of the resulting WSe_2 thin film[3]. The samples were prepared by an hour anneal at 900 °C with 130 ml/min flow of 5% hydrogen and 95% nitrogen gas[3]. The selenium source was heated to 340 °C and situated upstream of the samples[3].

Raman spectroscopy and X-ray Diffraction (XRD) data provided in the publication shows stronger WSe_2 peaks for samples deposited with an intermediate Ni_xSe_y film, meaning that the intermediate Ni-Se layer provides a more uniform substrate for higher crystallinity and texture of the WSe_2[3]. Also in the data is evidence of Ni_4Se_3 and $NiSe_2$ peaks in the Raman and XRD scans of the samples with intermediate layers[3]. Galen *et al.* also observed that an intermediate tin-selenium or indium-selenium layer allowed a decreased process temperature of 700 °C, indicating that the intermediate layer acts as a catalyst for the closest tungsten oxide molecules to form WSe_2[3].

Salitra *et al.* also utilized the selenization technique with the use of an open tube furnace and vacuum-evaporated WO_3 film on quartz[4]. Salitra *et al.* deposited 2000 angstrom films of tungsten oxide via vacuum evaporating powder WO_3 at 5 x 10^{-5} Torr using a deposition rate of about 10 angstroms per second[4]. They used a nickel-chromium coated and non-coated quartz substrate, where the metal coating was deposited by electron beam evaporation at about 10^{-6} Torr to a thickness of 200 angstroms[4]. The samples were introduced into the open furnace when it

reached a desired temperature of either 650 °C, 800 °C, or 900 °C depending on the experimental parameters[4]. The selenium source maintained a temperature of 300 °C in the inlet of the reactor, where it reacted with 100ml/min of forming gas (5% H_2 and 95% N_2)[4]. The sample was exposed to the forming gas and selenium vapor for an hour and then moved to an unheated zone to cool to room temperature[4]. A selenium atmosphere of 0.5 Torr was maintained throughout the whole process[4]. Salitra *et al.* discovered that this process produced the desired thin film of 2H hexagonal phase of WSe_2[4]. XRD data showed that the films grown on just quartz exhibited additional peaks of crystallites and poor grain structure, with average grain sizes of less than 100 Å and 300 Å for growth temperature of 800 °C and 950°C, respectively[4]. Scanning electron microscopy (SEM) displayed that the sample grown on quartz appeared amorphous with cracks in the film[4]. The WSe_2 grown on the Ni/quartz substrate demonstrated better crystallinity than the quartz substrate, however the lower growth temperature (650 °C) resulted with a poorly crystalline film[4]. Having a substrate with a Ni-Cr alloy intermediate layer produced greater adhesion and better crystallinity, though the intensity of the XRD data needed to be expanded by a factor of 150 for analysis[4].

1.2.2 Chemical Vapor Transport

Another technique used to synthesize WSe_2 is chemical vapor transport, in which source material of tungsten and selenium are sealed in a quartz ampoule under vacuum and heated to a temperature that allows the gaseous phase of the source materials to react and form WSe_2. The tungsten source might be tungsten trioxide, in which case selenization would occur, or another tungsten source. Additionally, a two zone furnace allows temperature gradients from the reaction

temperature to the growth temperature. Figure 1 depicts the general setup of chemical vapor transport.

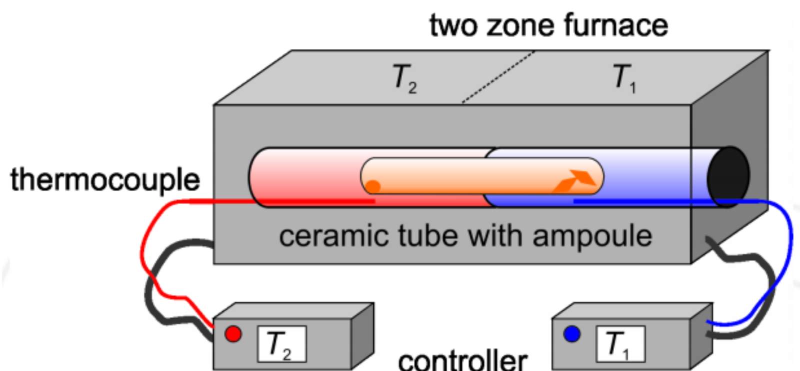

Figure 1. Experimental setup for chemical vapor transport[5]

Patel *et al.* used this technique to grow single crystal of WSe_2 and found that a reaction temperature of 1080 °C, a growth temperature of 1060 °C, a growth time of 240 hours, and a plate area of 6 mm^2 resulted in a highly crystalline WSe_2 single crystal[6]. Patel *et al.* used several characterization techniques like Energy Dispersive Analysis by X-ray (EDAX), XRD, and UV-VIS-NIR spectrophotometry to confirm the stoichiometry and crystal structure of the WSe_2[6]. This technique was successful for Patel *et al.* in creating large size single crystals and might not be an optimal process for thin film WSe_2 synthesis[6].

1.2.3 Powder Vaporization

Powder vaporization differs in the experimental setup from the chemical vapor transport method because the powder vaporization utilizes a horizontal furnace with carrier gas to carry vaporized source material over the sample substrate as opposed to sealed quartz tubes. Figure 2 shows the experimental setup for powder vaporization.

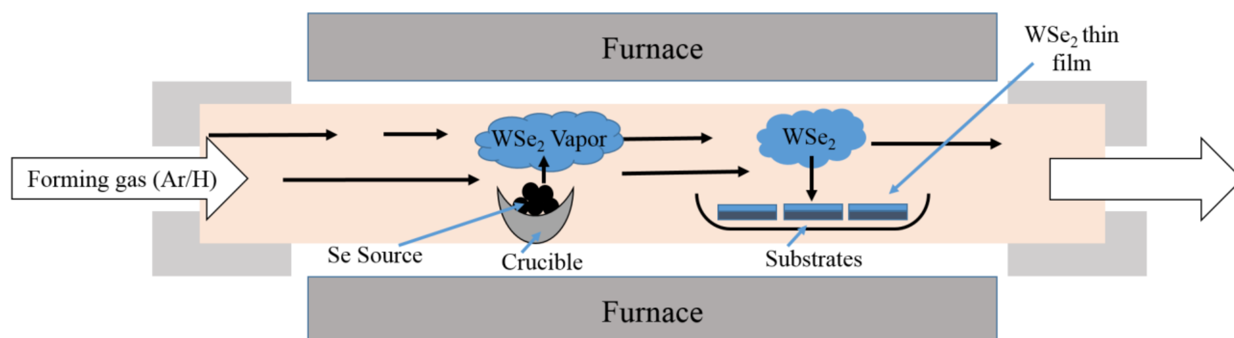

Figure 2. Experimental setup for powder vaporization

Clark and other colleagues utilized the powder vaporization technique to produce single-layered tungsten diselenide with high optical quality[7]. Tungsten diselenide triangles ranging up to thirty microns in edge length were formed on SiO_2 substrates[7]. Clark *et al.* placed WSe_2 powder into a crucible at a spot in the horizontal tube furnace that was heated to a temperature between 750 and 850 °C[7]. The SiO_2 substrate was placed in a spot in the furnace that was subsequently heated to about 940 °C at a rate of 35 °C/min[7]. The growth occurred for 5 minutes, during which 80 sccm of argon gas and 25 sccm of hydrogen gas flowed through the furnace with a pressure of about 5 Torr[7]. The samples were characterized using atomic force microscopy, optical microscopy, and photoluminescence. Clark *et al.* discovered that nearly perfect equilateral triangles formed with this procedure, suggesting uniform crystal quality and photoluminescence peaks corresponding with reported WSe_2 peaks from exfoliated WSe_2 monolayers[7].

1.2.4 Chemical Vapor Deposition

While chemical vapor transport has proven to produce large sizes of WSe_2, there is limited control on the reactant amount of WSe_2 forming on the substrate. For this reason,

chemical vapor deposition (CVD) offers more control of the flow of each precursor. Chemical vapor deposition differs in the experimental setup from the chemical vapor transport method because an open furnace is used to flow a constant supply of carrier gas during deposition. Carrier gasses, typically hydrogen, nitrogen or argon, flow over the selenium source and carries the vaporized selenium further down the chamber to a heated boat where powdered tungsten source sits next to the substrate. A chemical reaction occurs between the tungsten and selenium at the desired temperature and a layer of TMD material settles onto the substrate surface. Figure 3 shows the different mechanisms that occur over the sample surface during chemical vapor deposition.

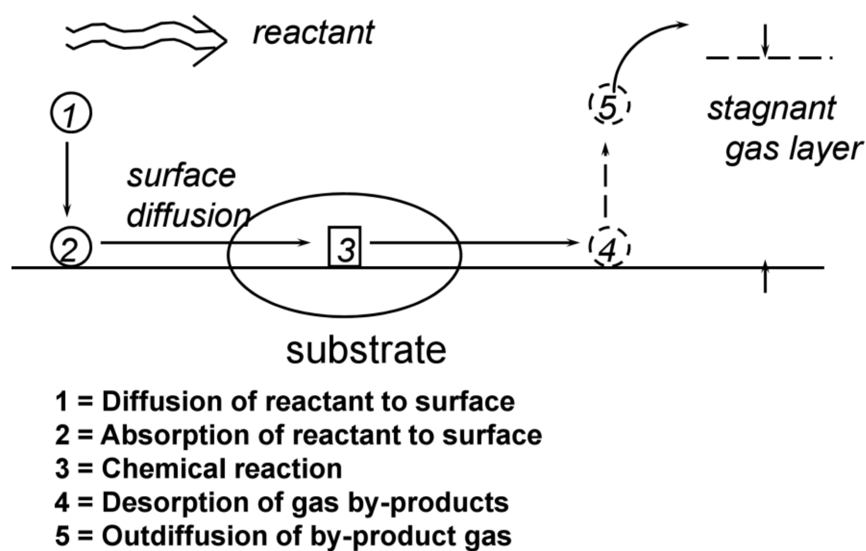

Figure 3. Growth mechanisms for chemical vapor deposition describe the interactions between reactant gasses and the substrate.[8]

As the reactant gas flows over the substrate, reactant particles diffuse to the surface, where they are absorbed[8]. Next the chemical reaction occurs that forms the WSe_2 thin film. Waste products from the reaction are subsequently desorbed and diffuse out of the substrate to be

pumped away from the chamber[8]. Figure 4 shows a general setup of a chemical vapor deposition system with the text rewritten verbatim to ensure clarity of the image.

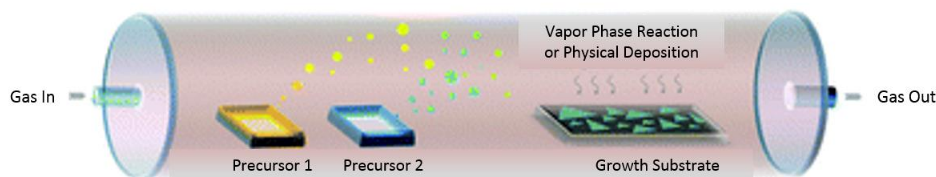

Figure 4. Chemical Vapor Deposition Setup[9]

CVD allows a wider window to change variables such as the precursor, temperature, amount of source material flown through, and pressure. Huang *et al.* used CVD to selenize WO_3 as their technique for WSe_2 thin film synthesis[10]. The research led to the understanding that the addition of hydrogen gas in the system could vastly improve the uniformity of the WSe_2 film[10]. Huang *et al.* flowed 80 sccm of argon gas and 20 sccm of hydrogen gas at a pressure of 1 Torr over a ceramic boat filled with selenium powders maintained at 270 °C, then passing over a separate ceramic boat filled with 0.3 grams of WO_3 powder[10]. The gas filled with Se and W vapor then flowed over the sapphire substrates, which were heated to temperatures ranging from 750 °C to 925 °C[10]. The growth process occurred for 15 minutes before the furnace was allowed to cool to room temperature[10]. The samples were then characterized by atomic force microscopy, Raman spectroscopy, optical absorption and photoluminescence. The sample grown at 850 °C exhibited monolayer WSe_2 triangles ranging from 10 to 50 micron in edge length[10]. Huang *et al.* speculated that the triangle size was limited by the lattice mismatch between the WSe_2 film and the sapphire substrate[10]. The sample grown at a temperature of 750 °C had much smaller triangles that merged together and had similar orientation[10]. This suggests an epitaxial growth mechanism of the triangles. Raman and photoluminescence confirmed WSe_2 growth and

distinguished monolayer from bilayer growth[10]. Because the chemical reactivity of selenium is very low, there needs to be a strong reducing agent like hydrogen to selenize the WO_3.

Chen *et al.* discovered that previous attempts of synthesizing WSe_2 via chemical vapor deposition failed largely on account to low reactivity of selenium[11]. They cited Huang *et al.*[10] who promoted using hydrogen gas as a reducing reactant to solve the issue. Chen *et al.* took the synthesis a step further to determine the growth mechanism of WSe_2 from this method[11]. Growth temperatures ranged from 875 to 900 °C for thin film growth, with 925 °C producing mostly thicker films[11]. Chen *et al.* used a horizontal CVD system in which the Si/SiO_2 substrate was placed with a quartz boat holding 40 mg of the tungsten precursor: WO_3 powder[11]. Powdered form of 30 mg of selenium and 5 mg of sulfur were placed in separate quartz boats that were located upstream of the substrate, with temperatures of 400 °C and 85 °C, respectively[11]. This allowed very minimal amounts of sulfur to sublime as the melting point of sulfur is above 85 °C at 115.2 °C[11]. Growth occurred for 12 minutes with a flow of 14 sccm Argon gas[11]. AFM and Raman was used to characterize the samples, and displayed a screw dislocation mechanism for WSe_2 growth[11]. The film was thicker than monolayer and showed some variation of thickness across individual triangles[11]. Raman data showed strong intensity, which suggest that the films are bilayer or thicker[11]. The multilayers of the triangles made evident the curved screw pattern of each subsequent triangle on top of the base triangle[11]. The downside to this growth mechanism is the limitation on lateral growth and layer by layer growth, which would produce more continuous films. Still, the WSe_2 film grown by Chen *et al.* was able to undergo e-beam lithography to fabricate a back-gated field-effect transistor, which performed favorably[11]. CVD exhibits other disadvantages as well, such as the inconsistency between an increased versatility at temperatures above 600°C and thermal instability of substrates at these higher temperatures[9].

Additionally, the vapor pressures of the precursors need to be high enough to vaporize the source material, which leads to the use of highly toxic precursors[9].

1.2.5 Metal Organic Chemical Vapor Deposition

A variation to the chemical vapor deposition technique described in Section 1.2.4 is known as metal organic chemical vapor deposition (MOCVD). Similar to chemical vapor deposition, MOCVD uses a carrier gas to flow vaporized precursors over a heated substrate, where the sources react and form a thin film. The sources for MOCVD, however, are metal organics and are typically introduced into the chamber as a gas source or as a vaporized source from solid or liquid precursors in a bubbler. For bubblers, the carrier gas is sent into the bubbler and the precursor vaporizes in accordance to its vapor pressure. The vaporized precursor is then sent through the gas lines into the chamber, where the synthesis reaction occurs. Figure 5 shows a bubbler schematic.

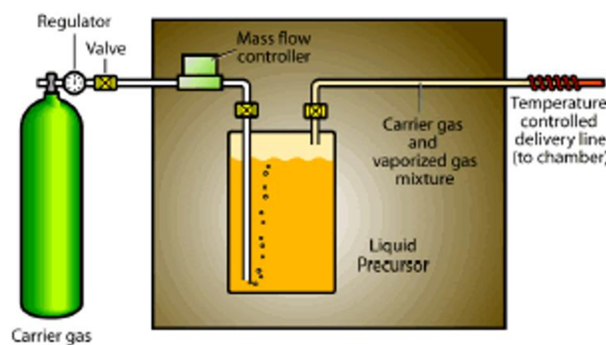

Figure 5. Schematic of a bubbler system[12]

The valves open and close according to a panel of manual switches that send a signal to a solenoid attached to air tubes. The tubes blast air into the valve to either open or close the line. Bubblers filled with precursors, either in liquid or powder form, can be cooled in a water bath or

heated by heat tape. The amount of precursor material that is vaporized is dependent on the amount of carrier gas that flows into the bubbler as well as the temperature of the bubbler. Higher temperature yields a higher concentration of precursor vapor. If the precursor is heated within the bubbler, heat tapes should be applied along the entire line leading to the chamber to make sure the precursor vapor does not cool and solidify in the gas line. Gas lines containing different precursor vapor are kept separate to reduce cross-contamination and chance of reaction. Once the gas lines reach the MOCVD chamber, the vapors of the tungsten and selenium sources are allowed to react onto the surface of the substrate, and waste gasses are pumped out of the system. The substrate lies on a susceptor that becomes heated through copper induction coils around the glass cylinder of the chamber. The amount of heat from the coils is determined by a power supply that is connected to a thermocouple. This thermocouple is fixed against the susceptor to maintain an accurate temperature reading, which is displayed on a temperature profile box. To make sure the glass cylinder stays cool enough and keeps from cracking, a second glass cylinder encases the chamber and a constant flow of cool water is sent between the two glass cylinders. Figure 6 shows a closer schematic of the MOCVD chamber.

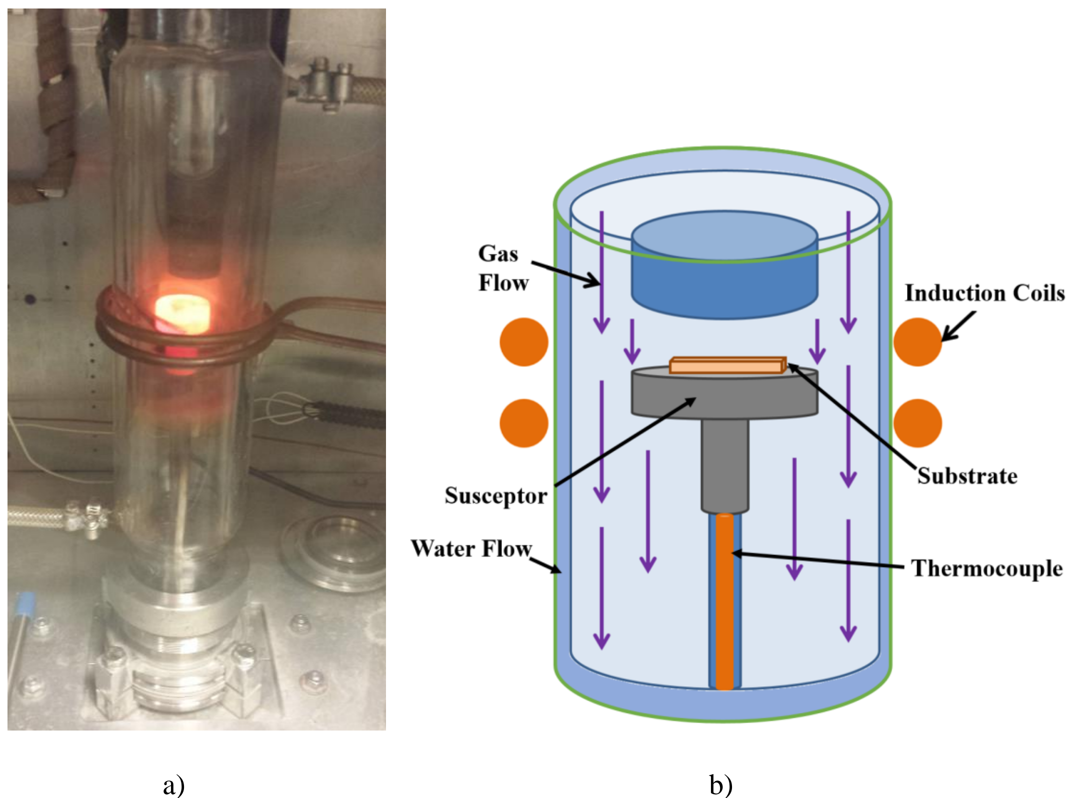

a) b)

Figure 6. The MOCVD chamber is set up to heat the substrate through induction heating on a susceptor. a) Image of MOCVD Chamber with heated susceptor; b) Schematic of the MOCVD Chamber

Figure 6a shows the induction coils around the middle of the glass cylinder, the water inlet at the top right of the chamber, and the water outlet at the bottom left of the chamber. As deposition occurs, the precursor vapors react and deposit both on the substrate and along the walls surrounding the heated susceptor, creating a dark film inside the inner glass cylinder. The MOCVD technique uses metalorganic precursors as the sources for tungsten and selenium. While these precursors have yielded high quality, crystalline WSe_2, the carbon in the methyl groups can be a possible source of carbon contamination that hinders the quality of the resulting thin films. Eichfeld, *et al*. successfully synthesized WSe_2 using MOCVD, and demonstrated atomically thin films with up to 8 micron domain size[13]. The advantage that this technique has over other synthesis methods is the ability to control numerous growth parameters like the

concentration of precursor that reaches the growth chamber and the duration of precursor exposure to the substrate, which ultimately increases the reproducibility for MOCVD experiments. Eichfeld, *et al.* reported that increased substrate temperature and chamber pressure increased the domain size of the tungsten diselenide at ranges of 700 °C – 900 °C and 500 Torr – 700 Torr[13]. This was observed on both epitaxial graphene and sapphire substrates[13]. Higher temperature also yielded higher particle density compared to lower temperature growths[13]. Transmission electron microscopy identified these particulates as excess tungsten, which suggests a deficient concentration of selenium during deposition[13]. Eichfeld and her colleagues then analyzed the effect of increased selenium concentration and observed an increase in triangle domain size as the Se:W ratio increased to 20,000, yet there was a limit to the ratio[13]. At a Se:W ratio of 100,000, the domain size decreased from five microns to less than a micron, with degraded triangle edges at the higher ratio[13].

1.2.5.1 Tungsten Precursors

Choosing the right precursor for the tungsten and selenium sources plays a key role in the reaction of WSe_2 within the MOCVD chamber. Lai and Lamb investigated tungsten hexacarbonyl as a source of tungsten[14]. For their experiment, Lai and Lamb deposited tungsten films on a silicon surface via chemical vapor deposition[14]. Tungsten hexacarbonyl is an ideal alternative to other tungsten precursors because it provides the ability for depositing highly pure metal films without damaging the dielectric layer beneath, which produces better films for device applications[14]. Lai and Lamb determined that a growth temperature below 500 °C allowed carbon and oxygen impurities into the film, which increased the resistivity, while growth

temperature of 500 °C or greater resulted in resistivities only 2-5 times greater than that of the bulk[14]. Annealing for an hour at 850 °C either in vacuum or with some forming gas lowered the resistivity and increased the purity of the tungsten film[14]. For deposition, 10 grams of tungsten hexacarbonyl [$W(CO)_6$] was loaded into the source tube and held under vacuum at 25 °C[14]. When the source is heated between 28-35 °C, the tungsten hexacarbonyl sublimes without any carrier gas according to the vapor pressure relation $\log_{10}P=12.094-4077/T$, with T in K and P in Torr[14]. If the source is heated between 80-150°C, then the vapor pressure responds as $\log_{10}P=11.523-3872/T$, with the same units as the previous equation[14]. Lai and Lamb maintained the source temperature between 65-70 °C[14]. Deposition occurred with a time between 1-20 minutes and a growth temperature between 350-600 °C[14]. Lai and Lamb determined that substrates must be heated to at least 350 °C in order for the tungsten to deposit onto the substrate[14]. Also, annealing the tungsten thin films under a vacuum at 900 °C for 30 minutes did not alter the composition any significant amount[14].

For the research described in this thesis, powdered tungsten hexacarbonyl was placed in a bubbler system. The bubbler temperature varied according to the run parameters and ranged from room temperature (23 °C) to 50 °C through the use of a heat tape. Because of this low temperature range, the partial pressure for $W(CO)_6$ was measured using the low temperature equation from Lai and Lamb: $\log_{10}P=12.094-4077/T$. Equation 2 details the calculation for determining the partial pressure of tungsten hexacarbonyl, which is a function of the bubbler temperature.

Equation 2. Partial Pressure of Tungsten Hexacarbonyl Precursor

$$W(CO)_6\ Partial\ Pressure = 10^{\left(12.094-\left(\frac{4077}{(W(CO)_6\ Temp[\circ C])+275}\right)\right)}$$

Using the partial pressure, the concentration of vaporized $W(CO)_6$ in standard cubic centimeters per minute (sccm) can be calculated, as shown in Equation 3.

Equation 3. Concentration of vaporized Tungsten Hexacarbonyl Precursor

$$W(CO)_6\ Concentration\,[sccm] = \frac{(W(CO)_6\,Partial\ \mathrm{Pr}essure[Torr]) \times (H_2\ Flow\ in\ Bubbler[sccm])}{Bubbler\ \mathrm{Pr}essure[Torr]}$$

1.2.5.2 Selenium Precursors

The corresponding component to the tungsten precursor is the selenium precursor. Mishra, Jeanneau, and Daniele experimented with dimethyl selenide as the source for their selenium-rich research[15]. Dimethyl selenide (DMSe) or $(CH_3)_2Se$ is a neutral organic compound that is considered to be the simplest possible selenoether. Mishra *et al*. utilized a metal organic chemical vapor deposition system under argon gas and vacuum line techniques[15]. For the purpose of their research, Mishra, Jeanneau, and Daniele combined the dimethyl selenide with anhydrous copper, gallium, and indium[15]. The complexes were then observed by elemental analysis Fourier transform infrared spectroscopy and nuclear magnetic resonance spectroscopy[15]. Low carbon content was reported after reacting with the other elements[13].

The dimethyl selenide precursor used for this thesis was purchased in a bubbler system though two companies, STREM and SAFC. The STREM source was only 99.0% purity, while the SAFC source was 99.999% purity. To calculate the concentration of vaporized DMSe in the MOCVD chamber, equations similar to the partial pressure equations in Section 1.2.4.1 were used. The partial pressure in Torr of the DMSe was a function of the bubbler temperature, as seen in Equation 4.

Equation 4. Partial Pressure of Dimethyl Selenium Precursor

$$DMSe\ Partial\ \Pr essure\ [Torr] = 10^{(9.872-(\frac{2224}{(DMSe\,Temp\,[\circ C])+273})}$$

This calculated partial pressure is then used to calculate the concentration of dimethyl selenium vapor that enters the MOCVD chamber, shown in Equation 5.

Equation 5. Concentration of Vaporized Dimethyl Selenium Precursor

$$DMSe\ Concentration\ [sccm] = \frac{(DMSe\ Partial\ \Pr essure[Torr]) \times (H_2\ Flow\ in\ Bubbler[sccm])}{Bubbler\ \Pr essure[Torr]}$$

Based on literature of WSe_2 synthesis, there are several techniques that successfully synthesize the transition metal dichalcogenide. Powder vaporization can produce highly crystalline WSe_2, yet the technique fails to control the precise amount of vaporized source material during synthesis. Chemical vapor transport yields highly crystalline, thick WSe_2 and so would not be a viable technique for thin film growth. Chemical vapor deposition offers more control of synthesis parameters than chemical vapor transport, yet metal organic chemical vapor deposition offers the most control of precursor vapor concentration and exposure to the substrate. MOCVD is an ideal technique compared to the other methods due to its precise control of growth parameters like precursor vapor concentration, pressure, temperature, and exposure time to each precursor.

1.3 Substrates for WSe_2 Growth

Because the tungsten diselenide is grown epitaxially, the interaction between the WSe_2 and the substrate upon which it’s grown is an integral parameter to analyze. Several common

substrates for semiconductor synthesis were analyzed for this research: sapphire, epitaxial graphene, and amorphous boron nitride. Each substrate material offers unique properties that affect the growth mechanisms for tungsten diselenide growth.

1.3.1 Sapphire

Sapphire substrates are widely used for semiconductor growth due to its optimal chemical stability, durability, radiation resistance, and other properties[16]. Sapphire is the single crystal form of the compound Al_2O_3, which is called corundum or alumina. Sapphire exhibits a hexagonal crystal structure with lattice constants or 4.785 Å and 12.991 Å[16]. Sapphire substrates are typically produced through three growth methods: Kyropolis, Bagdasarov, and Stepanov[17]. The Kyropolis method produces sapphire with high optical quality by using a thermic field and a lowered melt temperature to grow bulk crystal from a seed crystal of sapphire[17]. In the Bagdasarov method, the crystals form in a horizontal boat-shaped container, according to the mt-berlin website[17]. The sapphire is outputted as a slab, which can then be cut into thicker parts. The Stepanov method, or EFG, grows sapphire in argon or another inert gas[17]. The sapphire from this method is outputted as different and complex shapes like ribbons and rods[17]. The disadvantage with EFG is the presence of multiple crystallographic orientations, resulting in low optical quality of the sapphire[17]. Sapphire wafers are typically EPI-polished or optically polished before distribution[17]. The sapphire substrates used for this thesis research were greater than 99.998% LED Grade Sapphire purchased through Cryscore Corporation in wafers. These wafers were then cut by a diamond-tipped cutter into the sample size and subsequently cleaned via the cleaning process described in Section 2.1.

1.3.2 Graphene

Another substrate on which tungsten diselenide is synthesized is graphene, forming a heterostructure of two atomically thin materials. As the c-planes of both materials are dominated by van der Waals bonding, the combination of the two materials forms van der Waals heterostructures. Initial stages of heterostructure research saw the monolayers stacked via mechanical exfoliation, which can introduce contamination while transferring[18]. Even graphene synthesized by chemical vapor deposition on copper requires a post-synthesis transfer. Researchers, like Lin and his colleagues, began investigating synthetic approaches to forming WSe_2 on graphene to reduce the chance of contamination[18]. Lin *et al*. successfully grew high-quality WSe_2 monolayers directly on epitaxial graphene[18]. The epitaxial graphene used in this research is grown from silicon carbide (SiC) by subliming the silicon face of the SiC under argon gas at 200 Torr and 1725 °C. The WSe_2 synthesized by Lin *et al.* was then grown onto the epitaxial graphene using vapor phase transport technique at 925 °C to 1000 °C, with tungsten trioxide powder and argon/hydrogen carrier gasses and selenium vapor[18].

Lin and his colleagues determined that the epitaxial graphene offered a more conducive platform for the WSe_2 as opposed to the SiC base, as seen with the selective WSe_2 growth only on parts of the substrate that had epitaxial graphene[18]. This phenomenon can be explained by the different surface energies between graphene and silicon carbide, which alters the sticking coefficient of the materials.

1.3.3 Boron Nitride

Boron nitride is a compound consisting of alternating boron and nitrogen atoms bonded together. The arrangement of these two elements forms several different crystal structures: hexagonal, cubic, rhombohedral, and wurzite, but the boron nitride substrates used in this experiment were amorphous[19]. Because both boron and nitrogen surround carbon on the periodic table of elements, it stands to reason that the different structures of boron nitride share similar properties with carbon-based crystal structures like graphite and diamond. Boron nitride is known to be translucent, insulating with a high bandgap around 6eV, highly resistant to thermal shock from 2000°C-25°C, highly thermally conductive, highly chemically and thermally stable, and has a high compressive strength in the c direction[19]. These properties allow boron nitride to be a key building block for high-quality integrated electronics and photonics[19]. There are several techniques that can synthesize boron nitride thin films, each with a unique set of advantages and disadvantages. Common techniques of boron nitride synthesis are plasma sputtering, CVD, MOCVD, and atomic layer deposition[20]. The samples utilized for this research were prepared at 550 °C, with 50 mTorr pressure of nitrogen, and 100 laser pulses, which corresponded to about 10 nm – 15 nm thick boron nitride on sapphire. The samples were produced through a collaboration with Air Force Research Lab.

As described in the literature, the substrates on which WSe_2 is synthesized plays a role in the growth mechanism of the thin film. In in-depth analysis of each substrate utilizing a single synthesis technique is therefore necessary for understanding the true effect of these substrates on tungsten diselenide synthesis.

1.4 Motivation

Graphene made big news in recent years when it became the focus of the 2010 Nobel Prize in Physics by Andre Geim and Konstantin Novoselov[21]. A single layer of graphite, graphene contains electronic and optical properties that make it a viable material in numerous electronic devices[21]. To optimize the utility of graphene, the band gap, the energy difference between the conductive and valence bands, must be increased. To accomplish this, defects must be added to the graphene[21]. The band gap allows an "on/off" switch for electrical flow within electronic devices. This, however, has been incredibly difficult to achieve, leading to the search for materials that already have a sufficient band gap without defect addition. Scientists have recently begun focusing upon dichalcogenides like molybdenum disulfide (MoS_2) and tungsten disulfide (WS_2) since their electronic properties allow them to behave as both metals and wide-gap semiconductors[1]. Tungsten diselenide also promises optimal transport properties that make it a viable replacement for graphene[1]. As described, the applications for tungsten diselenide in electronic and optical devices have spurred several researchers to investigate ways to synthesize the thin film. With so many techniques to grow tungsten diselenide, a process-property analysis of the TMD is necessary for future scalable production. MOCVD, which allows precise control over a myriad of process parameters, is therefore an ideal technique to conduct the analysis. Like Eichfeld *et al*. described, the pressure, temperature, and precursor concentration effects on the film quality should be analyzed through several characterization techniques[13]. Atomic force microscopy of the samples can determine domain size, film thickness, particle density, and potential growth mechanisms. Raman spectroscopy can determine the atomic interactions and vibrational modes of the film to determine the material phase. Photoluminescence can confirm the presence of monolayer as opposed to multilayer through the interaction with light. Field

emission scanning electron microscopy can show the uniformity of the film. The process-property relationship is also determined by the substrate material, hence several substrates should be utilized.

1.4.1 Engineering Considerations

When addressing a scientific question, several consequences like economic, safety, environmental, and ethical effects must be addressed. Should the constraints on the project outweigh the potential benefits from the experimental results, then the research would be a detrimental contribution to the community. For this reason, several realistic engineering considerations were addressed in regards to this project. With regard to economic issues, synthesis of electronic materials can be a financial burden. Renting a single cylinder of hydrogen selenide gas as the selenium source is more than $5300. Powdered sources of material weighing 250 grams can cost a couple hundred dollars. The individual parts of the MOCVD system are pricey as well, with a single pressure controller costing almost $3000. Additionally the equipment used costs money to run. Even the characterization facilities like FESEM and Raman charge an hourly fee to utilize. The end goal of creating faster, more efficient devices justifies the huge economic burden. This research received the necessary funding from the Center for Low Energy Systems Technology (LEAST), which is a center under the STARnet phase of the Focus Center Research Program (FCRP), a Semiconductor Research Corporation (SRC) group funded by MARCO and DARPA.

Addressing the environmental impact of this research, several toxic chemicals are produced during the reaction, so strict procedures are enforced. The MOCVD system is carefully

leak checked after any adjustments to the gas manifold, and the system is brought to a pressure of 10^{-3} Torr before any growth to ensure an airtight system. Additionally, the MOCVD system sits within a vented cabinet with a strong exhaust to remove any potential gasses that might leak from system. By-products from the synthesis are pumped out of the system into a scrubber, which measures the pH of the waste and mitigates with either sulfuric acid or potassium permanganate to balance the pH before the waste is exhausted to the building exhaust. Residual waste product inside the liner tube is cleaned with nitric acid, and the waste from this cleaning process is properly disposed of into labeled and vented waste containers.

With the environmental impact comes an impact on the health and safety of the user and other lab members. Proper personal protective equipment (PPE) is enforced during every step of the synthesis process, and lab members are encouraged to remind other members if PPE is not followed. The gas cylinders in use are stored in vented gas cabinets to confine any potential leaks. Additionally, these gas cabinets are attached to the building alarms, so any potential leaks in the lab are alerted to lab users throughout the building. An efficient emergency evacuation procedure is practiced and enforced, so that lab users exit the building quickly and safely. Several pump purge steps, described in Section 2.2, are required after each growth in the MOCVD system to remove the risk of exposing the user to harmful by-products. Additionally, the earlier-mentioned scrubber reduces the risk of contaminating the building exhaust, which affects other lab users in the building. The standard operating procedures for each process of the synthesis is readily accessible in the lab, and lab members are encouraged to reference these procedures.

As for the social, political, sustainability, and manufacturability constraints, this research strives to provide the fundamental layer of semiconductor material upon which devices are

fabricated. If successful, tungsten diselenide can produce more efficient devices than graphene and silicon. As most devices currently are silicon-based and exhibit limited efficiency, using WSe_2 can result in future electronics that utilize much lower power consumption. Reducing power consumption has the ability to affect society in both a governmental and commercial setting. Additionally, the scalable and reproducible nature of metal organic chemical vapor deposition allows a faster transfer to commercial manufacturing of devices.

CHAPTER 2

PROCEDURE

2.1 Substrate Cleaning Procedure

The preparation of the substrates before synthesis is crucial to prevent defects and contamination on the resulting tungsten diselenide thin films. Substrates for this experiment are prepared with a standard wet cleaning procedure. Some substrates arrive in wax, so these substrates should be submerged in Opti-clear, a commercial cleaning agent, overnight and then rinsed in deionized water before conducting the standard wet cleaning procedure. The first step of the standard wet cleaning procedure is to submerge the substrate in acetone solution and ultrasonicate the solution for ten minutes. Then the substrate is quickly transferred to a beaker of isopropyl alcohol (IPA) solution and ultrasonicated once more for ten minutes. The sample is then transferred to a beaker of deionized water, which is subsequently rinsed at least three times. Next the substrate is placed in a beaker of acidic nanostrip that is heated on a hot plate to 80 °C

for 20 minutes. Additional personal protective equipment (PPE) is necessary when handling nanostrip, which is a mixture of sulfuric acid and hydrogen peroxide. The sample is then carefully transferred to the beaker of deionized water and rinsed at least fourteen times to remove residual nanostrip. Finally, the substrate is dried with a nitrogen gun to keep water from drying upon the surface. Additionally the substrate can be exposed to oxygen or argon bombardment to further remove particulates from the surface. This oxygen or argon etching technique is conducted in an etching machine like a PT 720 machine.

2.2 Deposition System Preparation and Safety

The furnace system must be prepared before every synthesis to ensure each growth is conducted under uniform conditions. To turn on the metal organic chemical vapor deposition (MOCVD) system, the external pump system must first be turned on. This pump removes the waste vapors that flow through the chamber of the furnace in a chemical scrubber. The scrubber measures the pH of the waste and mitigates with either sulfuric acid or potassium permanganate to balance the pH before the waste is exhausted to the building exhaust. Next, the MOCVD system needs a direct path for nitrogen gas to flow through the system and into the pump. The MOCVD system is attached to a pressure gauge that controls a butterfly valve, which determines the flow into the pump and hence the pressure inside the furnace chamber. When the furnace is not in use, the pressure in the chamber should be set to atmospheric pressure with only nitrogen gas as a safety precaution against any pressure build-ups or system leaks. To turn off the system after use, close the hydrogen gas cylinder in the gas cabinet, purge out the hydrogen line to at least 2.5 E-2 Torr, pump purge the system, bring the chamber to atmospheric pressure with

nitrogen, turn any heat tapes off, close the water valves and the nitrogen dilution, and turn off the remaining switches.

The pump purge process is necessary to force residual gas from the previous growth through the system and into the pump as waste. The "pump" portion of the process involves filling the chamber up to 100 Torr of nitrogen gas. The "purge" portion then expels this gas along with any gas that remained in the system. A purge is executed directly after a run to expel the waste gases before a pump is executed.

The first step to purging the MOCVD system is to close the valves to any gas or bubbler lines. The only valves open should be connecting lines previously used to the pump as long as no gas or bubbler source is connected to the chamber. The butterfly throttle valve should then be opened, as well as the bypass valves, which often trap gasses. The chamber pressure should read at most 10 E-3 Torr on the Purani gauge in order to properly purge the system. The bypass valves should then be closed, leaving only the valves to lines where nitrogen can pass through. To pump the MOCVD system, a direct line should be open to allow nitrogen gas to flow into the chamber. The butterfly throttle valve should then be closed to fill the chamber pressure to at least 100 Torr under nitrogen. After the chamber pressure reaches 100 Torr, the butterfly throttle valve should be opened and the valve to the nitrogen gas line should be closed. The pump purge process should be repeated three times to ensure the removal of residual waste and gasses. After the final purge to 10 E-3 Torr, the nitrogen gas line valve should be opened and the chamber pressure should reach atmospheric pressure using the pressure set points.

As mentioned in the description of the MOCVD system, liner tube provides a barrier from the reaction chamber and the outer glass structure of the chamber, allowing water to flow between the glass tubes to keep the chamber from melting with the coils' heat. The liner tube

should be replaced every two or three depositions of the same precursors because residues build up along the walls. To clean a liner tube, place the tube in a graduated cylinder filled with 200 mL of nitric acid under the fume hood, cover the top of the inner glass cylinder with aluminum foil, and allow the nitric acid to clean the residue overnight. The next day, the nitric acid can be rinsed off following proper safety precautions, and the liner tube can be dried for the next use.

When operating the system with hydrogen, a nitrogen dilution must enter the gas as it travels to the scrubber to maintain a safely diluted hydrogen level. To open the hydrogen gas cylinder, the manual knobs must be opened in the gas cabinet, opening first the cylinder and working through the line to the MOCVD system valve. The gas purifier in the cabinet can be a fire hazard if hydrogen gas is purged out, so opening the line from the gas cylinder outwards is necessary. Also necessary is a constant flow of water along the glass chamber tubes to keep the chamber from melting under the heat from the copper coils. The water line is opened by opening the inlet and outlet lines simultaneously and slowly opening the bypass line to allow water to flow through the system.

To further remove contaminations within the MOCVD chamber, a hydrogen bake is conducted without any substrate or exposure to precursors. The hydrogen bake should reach a temperature well above the temperature during deposition to ensure no residual waste will react during the subsequent deposition. The temperature program controller can then be set to ramp the temperature to 900 °C at 80 °C/min and dwell at that temperature for 20 minutes until cooling down to room temperature at 225 °C/min. Mass flow controllers should be adjusted to flow 430 sccm of hydrogen directly through the system. Use the pressure controller to set the chamber pressure to 100 Torr and allow the hydrogen gas to pressurize the chamber. Once the

bake is completed, the hydrogen valve should then be closed and the system should be pump purged.

2.3 WSe_2 Synthesis via Metal Organic Chemical Vapor Deposition

A cleaned substrate will be placed in the chamber of the metal organic chemical vapor deposition (MOCVD) system. Hydrogen gas will act as a carrier gas through two bubblers filled with tungsten hexacarbonyl ($W(CO)_6$) and dimethyl selenium ($(CH_3)_2Se$ or DMSe), respectively, which in turn sends $W(CO)_6$ and DMSe vapor over the sample. As the MOCVD system is heated up, the dimethyl selenium reacts with the flow of tungsten hexacarbonyl gas and settles on the substrate, resulting in a WSe2 thin film sample. A hydrogen anneal is conducted with the substrate in the system but without any precursor exposure to further clean the chamber from water. Directly after the anneal, the substrate is heated to the growth temperature, and the bubblers are open to allow deposition. Bubblers should be open only when the chamber has reached the desired deposition temperature and should be kept open only during the desired growth time. This controls the amount of vaporized precursor in the chamber to maintain reproducibility of runs. Figure 7 below shows the temperature profile for a typical deposition of WSe_2.

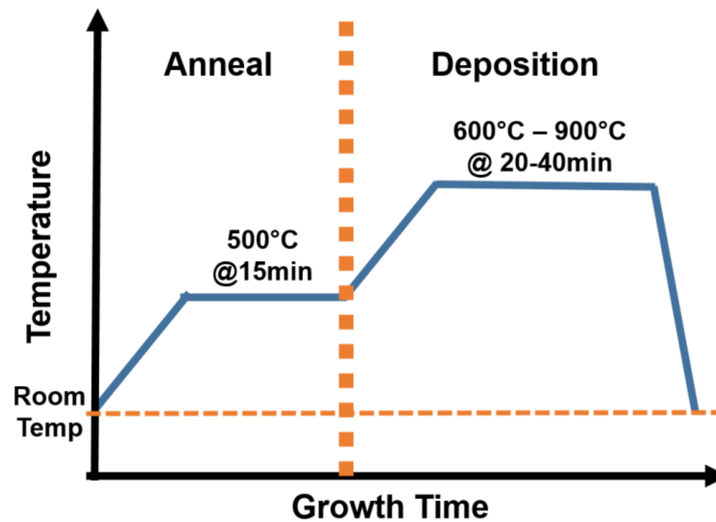

Figure 7. Temperature profile of WSe_2 deposition via MOCVD

After cooling the system and purging out the reaction waste, the WSe_2-covered substrate is removed to analyze its properties.

2.4 Data Analysis

Once the samples have been grown, a surface study can be conducted using characterization tools such as Raman spectroscopy, photoluminescence, atomic force microscopy, and field emission scanning electron microscopy. The combination of these techniques will be able to provide ample information about the sample surfaces that will then be correlated with the devices' electronic properties.

2.4.1 Raman Spectroscopy

Raman spectroscopy will examine the chemical, structural, and optical properties of the surface to confirm the presence of WSe2 on the sample. The Raman spectrometer shines a laser at the sample. This light interacts with the molecules on the sample surface, which shifts the energy of the laser light. The inelastic scattered light is then collected by a lens and passed through a monochromator that determines the wavenumber of the light by its change in energy and displays the data as a graph of intensity versus wavenumber. By comparing intensity peaks given from the sample to accepted peaks of known compounds and elements, the composition at the surface of the sample can be determined. WITec Project software was used for the Raman data. Sapphire samples were analyzed under a 633nm laser to reduce laser damage to the surface. Additionally, laser wavelengths affect the prominence of peaks, and 633nm provided a clear distinction of the A_{1G} and E_{2G} peaks compared to a 488nm laser. Samples grown on epitaxial graphene or boron nitride were analyzed under the 488nm laser, however, as these samples were more robust compared to sapphire under the laser. An integration time of 20 seconds, a hard number of 5, and a soft number of 1 allowed a thorough scan time. These values determine how long the sample is exposed to the laser to record the emission spectra.

Typical Raman peaks for WSe_2 represent the vibrational modes of the TMD, E_{2G} for in plane vibrations and A_{1G} for our of plane vibrations[22]. Table 1 shows the common peaks visible in a WSe_2 Raman spectra[22].

Table 1. Common Peaks in WSe_2 Raman Spectra

Wavenumber	Vibrational Mode
138 cm^{-1}	A_{1G} + LA of WSe_2

248 cm^{-1}/258 cm^{-1}	E_{2G}/A_{1G} of WSe_2
378 cm^{-1}	E_{1G} +LA of WSe_2
502 cm^{-1}	$2E_{1G}$ of WSe_2
625 cm^{-1}/740 cm^{-1}	Higher order modes of WSe_2
1370 cm^{-1}/1400 cm^{-1}	Sapphire
1600 cm^{-1}	D/G peak of Carbon

Seeing a peak at 1600 cm^{-1} on a WSe_2 sample means that carbon contamination is present on the surface, which will hinder the film's effectiveness as a device. Figure 8 shows a typical Raman spectra for tungsten diselenide on a sapphire substrate.

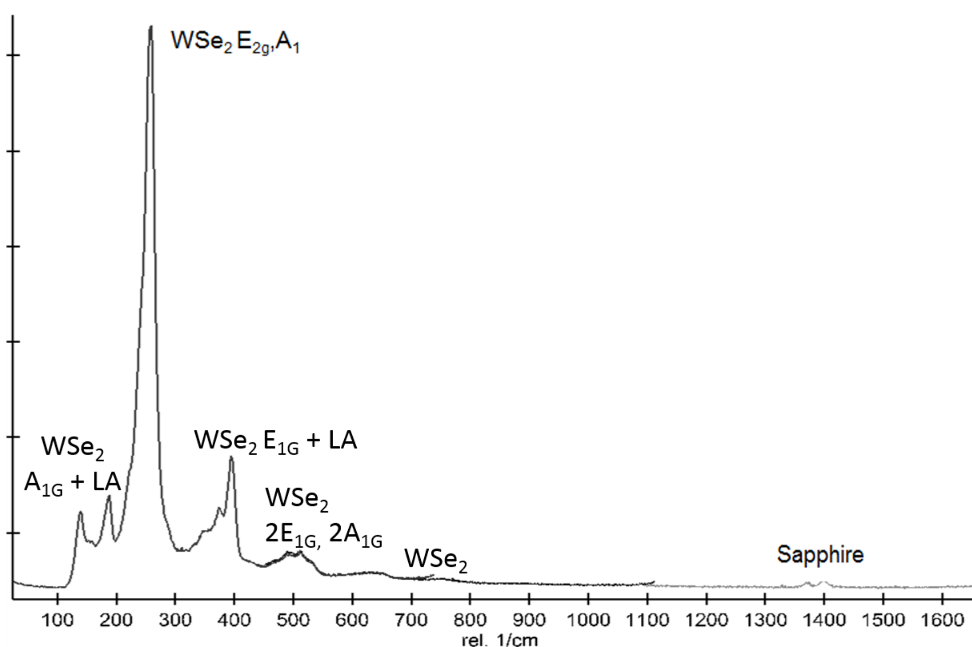

Figure 8. Typical Raman Spectra for WSe_2 on Sapphire Substrate

This sample does not vibrate at the wavenumber representative of carbon, which means that there was not carbon at the scanned location.

2.4.2 Photoluminescence

Photoluminescence (PL) uses photon excitation to determine the purity and crystalline properties of the samples. Figure 9 below shows a schematic of photoluminescence analysis.

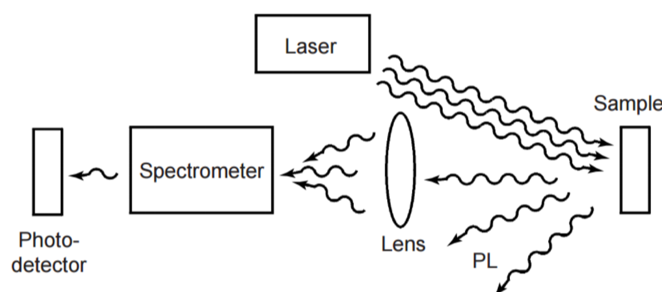

Figure 9. Experimental Setup of Photoluminescence Measurement[23]

After the laser bombards the sample with photons, a photodetector can pick up the emitted PL wave. High intensity peaks correspond to photon-induced excitation of the sample that result in radiative relaxation of the electrons to the ground state[23]. Samples with bulk thickness fail to exhibit a photoluminescence signal. The width of the PL peak correlates the quality of the material, with a narrow peak meaning a more responsive material to photo-excitation. Additionally, a shift in the peak position from literature value suggests doping and straining of the material. Monolayer tungsten diselenide typically has a PL peak around 1.65 eV. This peak shifts and widens as the thin film becomes bilayer or multilayer. Thick tungsten diselenide fails to exhibit a PL peak. Figure 10 shows the literature-reported photoluminescence peaks for monolayer, bilayer, and bulk tungsten diselenide[2].

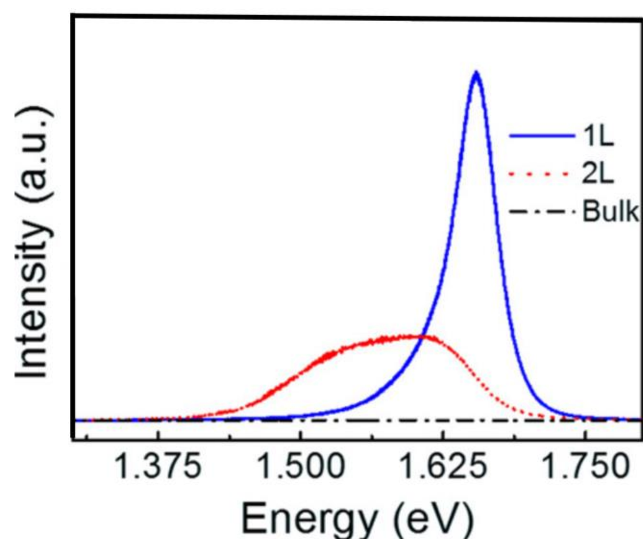

Figure 10. Photoluminescence signals from monolayer, bilayer, and bulk WSe_2[2]

Using a sapphire substrate results in two sharp peaks in the PL around 1.78 eV and 1.79 eV. A monochromatic laser of 488nm was used for photoluminescence measurements, with an integration time of 5 seconds, a hard number of 4, and a soft number of 1.

2.4.3 Atomic Force Microscopy

Atomic force microscopy (AFM) will examine the surface morphology and roughness of the samples to determine if the sample has a continuous film. AFM uses a piezoelectric tip that vibrates at a specific height. When the tip comes into contact with a surface, the AFM measures how much the tip was supposed to move in comparison to the actual movement due to the surface roughness, and records the difference as the height of the sample. NanoScope software was used to collect and analyze the atomic force microscopy data. Typical scan sizes were 2 microns by 2 microns with 512 lines for higher resolution of scanning.

2.4.4 Field Emission Scanning Electron Microscopy

Field emission scanning electron microscopy (FESEM) uses a voltage and electron bombardment to create an image of a sample surface. A field emission source free the electrons and gives rise to the name of the technique[24]. Secondary electrons are emitted from the sample surface after electron bombardment, and these secondary electrons travel at a velocity determined by the levels and angles at the sample surface[24]. The secondary electrons then collide with a mirror in the FESEM machine that fluoresces to produce photons[24]. The photons are transduced to a video signal and sent through a cathode ray tube in synch with the electron beam movement over the sample[24]. An image is then produced that shows topological contrast of the sample surface[24]. Higher spatial resolution and minimized charging and damage on the sample makes FESEM an optimal characterization technique compared to regular scanning electron microscopy[24]. The FESEM images taken provide insight about surface interactions that may not be visible in AFM images. Additionally, FESEM allows a wider area to be observed at a quicker scan time than AFM images.

CHAPTER 3

RESULTS AND DISCUSSION

3.1 Preparation Study

The preparation study was conducted on three sapphire substrates. After each sample was standard wet cleaned, one sample was given an additional oxygen etch, another was argon

etched, and the third sample was left with just the standard cleaning procedure. All three of these samples were placed in the MOCVD system for a simultaneous growth to ensure that all deposition parameters were consistent. The AFM images of the samples after growth are displayed in Figure 11 below.

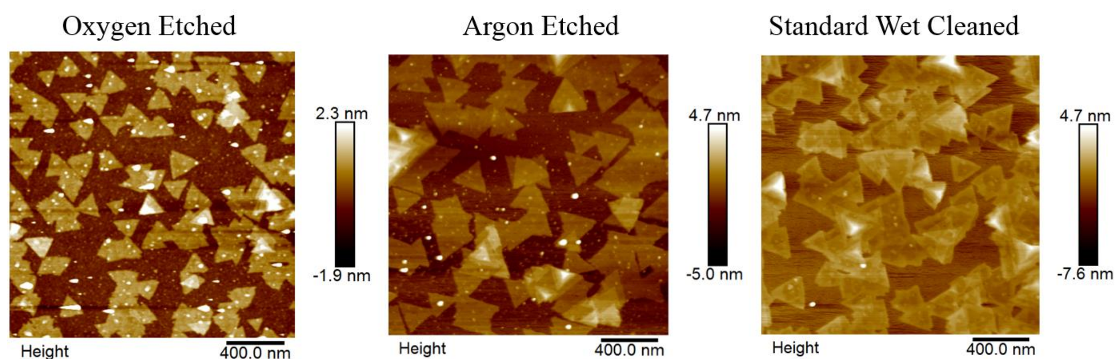

Figure 11. AFM images of sapphire substrates cleaned via standard wet cleaning or addition oxygen or argon etching demonstrate no increase of domain size (300 nm) compared to standard process.

As seen in Figure 11, there was no distinct change in triangle domain size with each cleaning technique. Additionally, the particle density for the two etched samples increased from 20 particles/μm^2 for the standard cleaning to 150 particles/ μm^2 and 100 particles/ μm^2 for the oxygen and argon etched, respectively. A possible explanation to the increased particle density is that etching removes dangling bonds on the surface, which reduces the reactivity of the substrate. This causes more precipitates to form instead of WSe_2 coupling with the substrate. The standard wet cleaning procedure was consequently utilized for the remainder of the samples in this research.

3.2 Tungsten Diselenide on Sapphire

Synthesizing tungsten diselenide on sapphire substrates took many growths before any monolayer triangles were produced, as the majority of samples in the beginning of the research exhibited thick, nanocrystalline WSe_2 films. The first study analyzed was the effect of reducing the sample's exposure time to the tungsten precursor. Sapphire substrates in the study were exposed to 30 minutes of dimethyl selenium precursor at 775 °C. After five minutes of selenium deposition, sample A was exposed to the tungsten hexacarbonyl, which remained open for the remainder of deposition. Sample B was exposed to the tungsten precursor after 10 minutes of selenium deposition, sample C was exposed with 15 minutes left of deposition, and sample D was exposed to the tungsten hexacarbonyl after 20 minutes of selenium deposition. Figure 12 shows a graph of the growth runs.

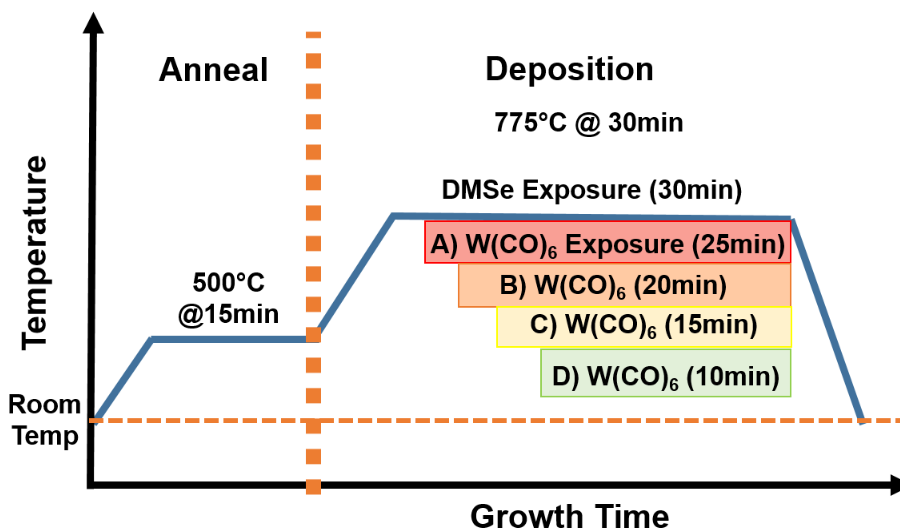

Figure 12. Profile of Tungsten Hexacarbonyl Exposure Time Study

The deposition temperature remained constant at 775 °C, and the only variable changed between samples was the time allotted for the tungsten hexacarbonyl bubbler to be open to the MOCVD chamber. Figure 13, below, the resulting AFM of these samples.

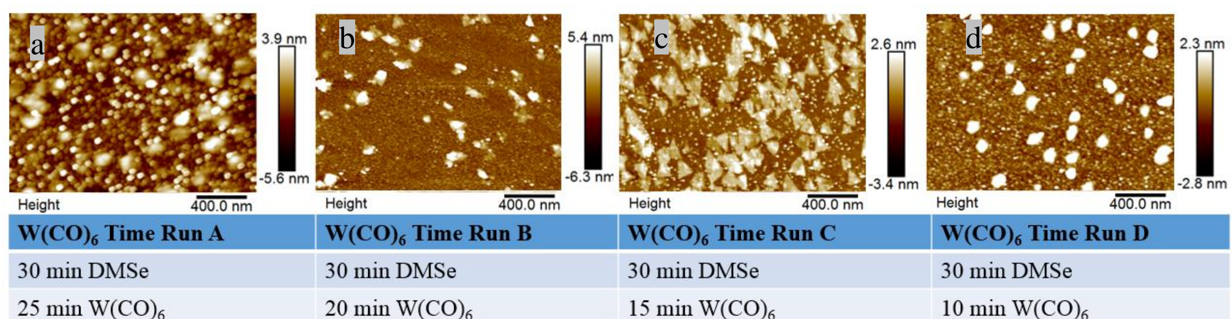

$W(CO)_6$ Time Run A	$W(CO)_6$ Time Run B	$W(CO)_6$ Time Run C	$W(CO)_6$ Time Run D
30 min DMSe	30 min DMSe	30 min DMSe	30 min DMSe
25 min $W(CO)_6$	20 min $W(CO)_6$	15 min $W(CO)_6$	10 min $W(CO)_6$

Figure 13. Varying exposure time of the tungsten source affected the nucleation and particle density of the WSe_2.
a) 25 min $W(CO)_6$; b) 20 min $W(CO)_6$; c) 15 min $W(CO)_6$; d) 10 min $W(CO)_6$

As seen in Figure 13, the domain size of the WSe_2 triangles increased to 300nm for sample C with 15 minutes of tungsten hexacarbonyl exposure, which is larger than the 100nm triangles in sample A. Also, the size of the particulates decreased from 20 nm to 5 nm as the duration of tungsten precursor was decreased. This decrease in particle size as less tungsten is introduced inside the chamber suggests that there is an excess in tungsten in the system. Excess amounts of tungsten compared to selenium hinder the domain size and nucleation of triangles.

Next, the temperature dependence was analyzed. Samples were grown at 700 Torr with a pre-deposition anneal at 500 °C for 15 minutes. The ratio of selenium precursor vapor in the system to tungsten precursor vapor was 700 for these samples. Figure 14 shows the temperature profile for these samples.

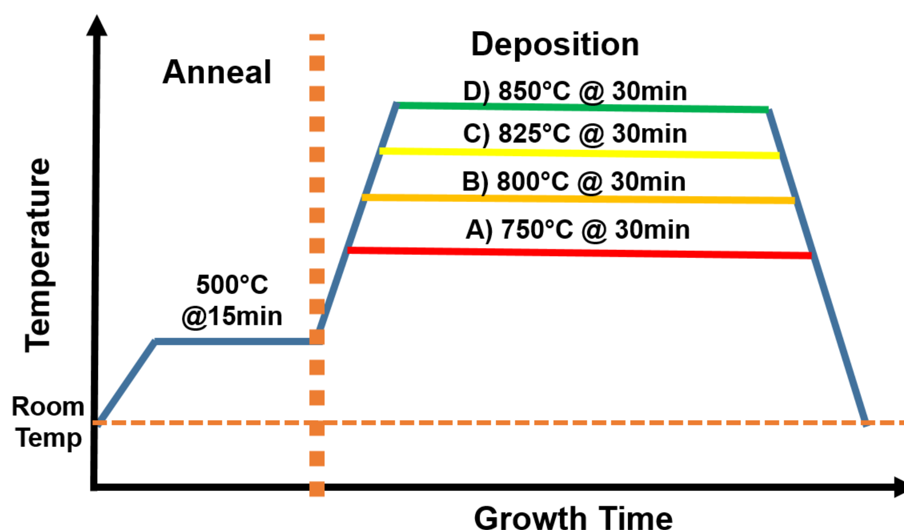

Figure 14. Temperature Profile for WSe_2/Sapphire at Varying Temperatures

After synthesis, the samples were analyzed via atomic force microscopy, as shown in Figure 15.

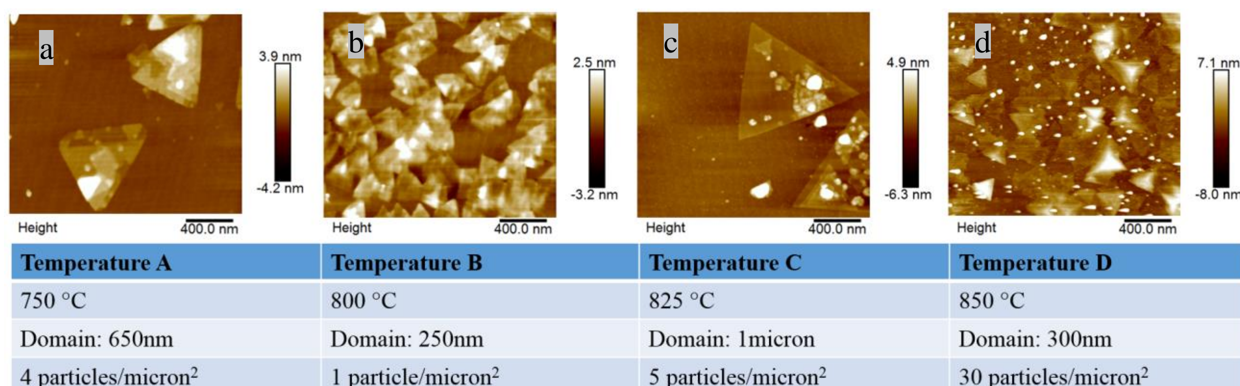

Temperature A	Temperature B	Temperature C	Temperature D
750 °C	800 °C	825 °C	850 °C
Domain: 650nm	Domain: 250nm	Domain: 1micron	Domain: 300nm
4 particles/micron^2	1 particle/micron^2	5 particles/micron^2	30 particles/micron^2

Figure 15. AFM images of samples grown at 750 °C, 800 °C, 825 °C, and 850 °C demonstrate increased domain size from 650nm to 1 micron

The sample grown at 825 °C had 1 micron triangles, which was larger than the 650nm triangles on the sample grown at 750 °C. This domain size decreased at 850 °C to a mere 300nm, however. Raman spectra of these samples confirmed the presence of WSe_2, as seen in Figure 16.

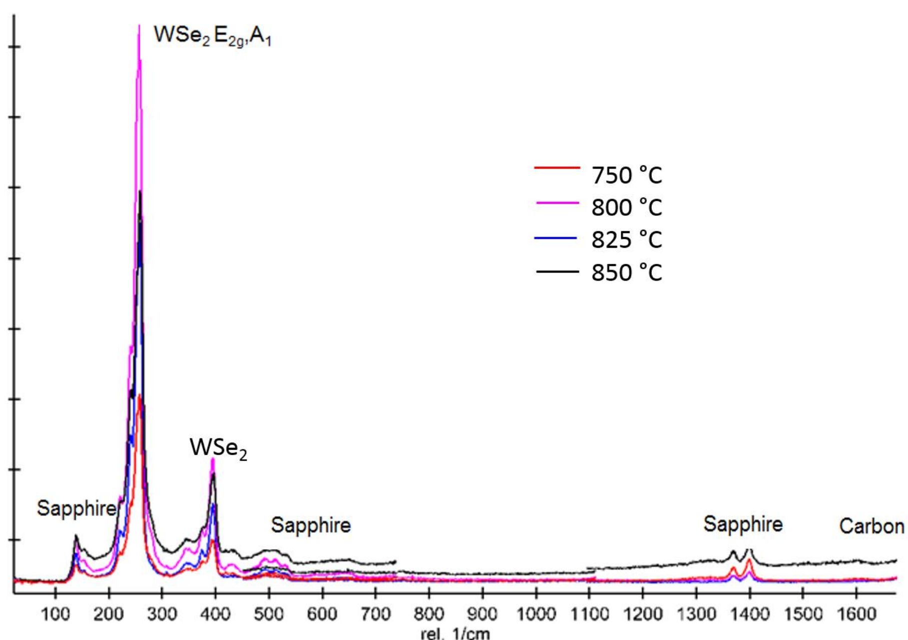

Figure 16. Raman spectra for WSe_2/Sapphire samples grown at different temperatures

The samples exhibited high intensity peaks corresponding to the A_{1G} and E_{2G} vibrational modes of WSe_2[22]. The high temperature sample at 850 °C exhibited carbon peaks, which could explain the decrease in domain size of the WSe_2. Carbon contamination hinders the nucleation of tungsten diselenide.

The next parameter to be analyzed was the ratio between selenium precursor vapor concentrations and tungsten precursor vapor concentrations. These runs were conducted at 800 °C for 30 minutes with a pressure of 700 Torr. Figure 17 shows the resulting AFM images from these runs.

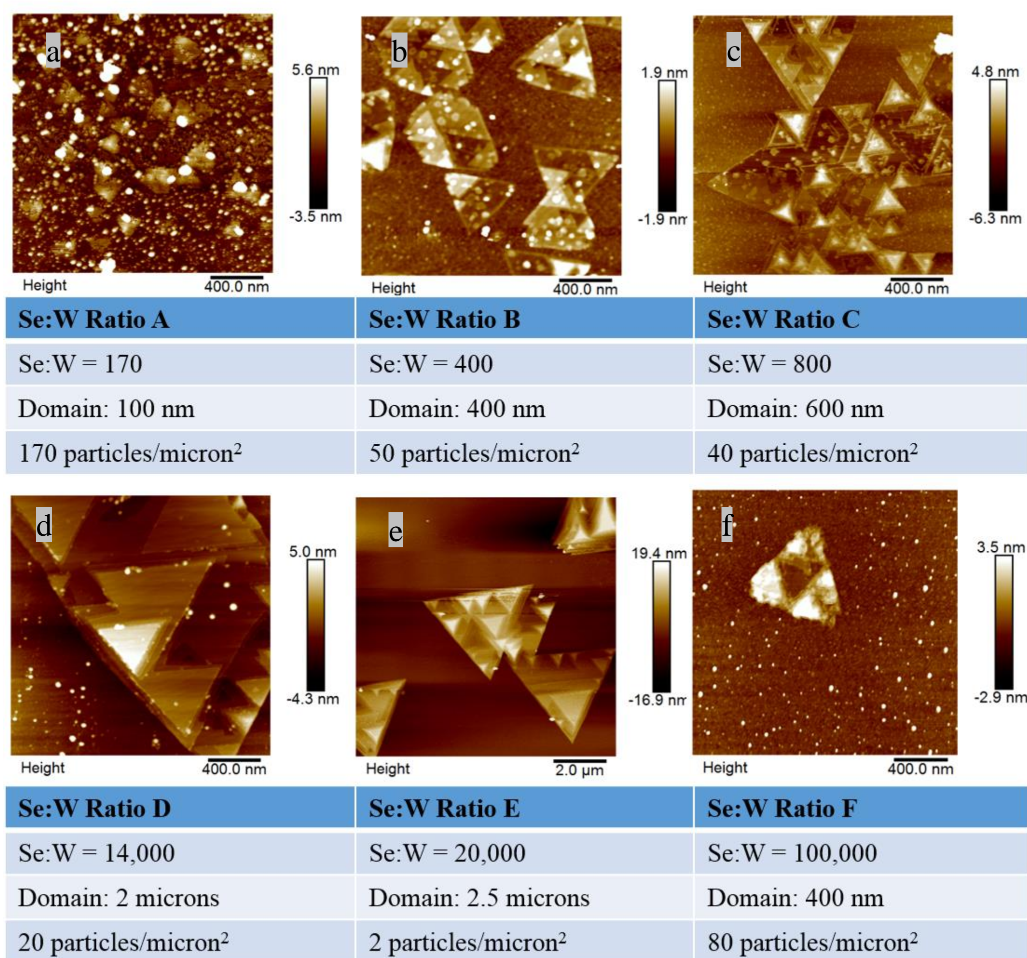

Se:W Ratio A	Se:W Ratio B	Se:W Ratio C
Se:W = 170	Se:W = 400	Se:W = 800
Domain: 100 nm	Domain: 400 nm	Domain: 600 nm
170 particles/micron^2	50 particles/micron^2	40 particles/micron^2

Se:W Ratio D	Se:W Ratio E	Se:W Ratio F
Se:W = 14,000	Se:W = 20,000	Se:W = 100,000
Domain: 2 microns	Domain: 2.5 microns	Domain: 400 nm
20 particles/micron^2	2 particles/micron^2	80 particles/micron^2

Figure 17. AFM images of WSe_2/Sapphire with varying Se:W ratios. a) Se:W = 170; b) Se:W = 400; c) Se:W = 800; d) Se:W = 14,000; e) Se:W = 20,000; f) Se:W = 100,000

As displayed in Figure 17, higher concentrations of selenium vastly improve the domain size of the WSe_2 from 100nm to 2.5 microns in size. There is a limit to the ratio, for when the selenium concentration is too high (Se:W 100,000), the domain size decreases to 400nm and the number of particulates increases to 80 particles per square micron. On a similar trend as the domain size, the particle density on the sample surface decreases with increasing Se:W ratio, with an apparent limit at a Se:W ratio of 100,000. This decrease in particle density with increasing selenium concentration relative to the tungsten concentration suggests that particles are tungsten-rich particles due to selenium deficiencies. A Se:W ratio of about 20,000 is optimal

with few particulates (2 particles per square micron), and a 2.5 micron domain size. Additionally, the total flow of hydrogen in the MOCVD system affects the domain size. Two runs were done at 700 Torr, with an anneal time of 15 minutes at 500 °C, a growth time of 30 minutes at 800 °C, and a Se:W ratio of 15,000. The difference between the runs was the total flow rate of hydrogen: 100 sccm versus 250 sccm, where sccm is standard cubic centimeters per minute. Figure 18 shows AFM images comparing the two samples.

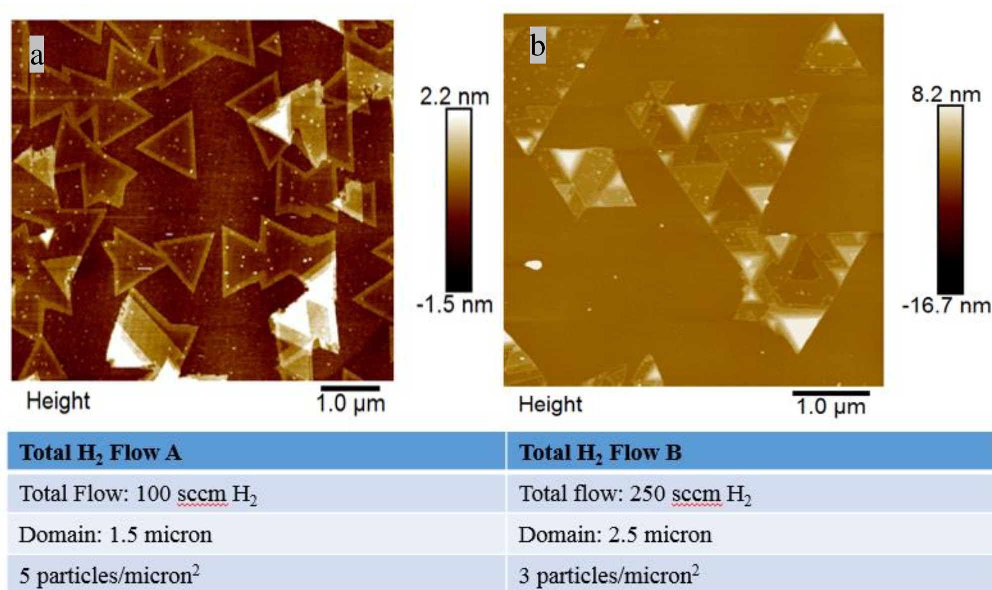

Total H_2 Flow A	Total H_2 Flow B
Total Flow: 100 sccm H_2	Total flow: 250 sccm H_2
Domain: 1.5 micron	Domain: 2.5 micron
5 particles/micron^2	3 particles/micron^2

Figure 18. AFM of WSe_2/Sapphire synthesized at different total hydrogen flow rates shows an increase in domain size as total flow increases.
a) Total flow = 100 sccm H_2; b) Total flow = 250 sccm H_2

Figure 18 shows that increasing the flow rate of hydrogen in the system from 100 sccm to 250 sccm increases the domain size of the WSe_2 triangles. The flow rate increases the growth rate of the reaction between the precursors, which favors lateral growth of the triangles.

3.3 Tungsten Diselenide on Epitaxial Graphene

Epitaxial graphene exhibited much higher domain sizes compared to sapphire samples synthesized at lower Se:W ratios. Figures 19 and 20 are testament to this observation. Figure 19 shows a temperature study of WSe_2 on epitaxial graphene, grown at a Se:W ratio of 170.

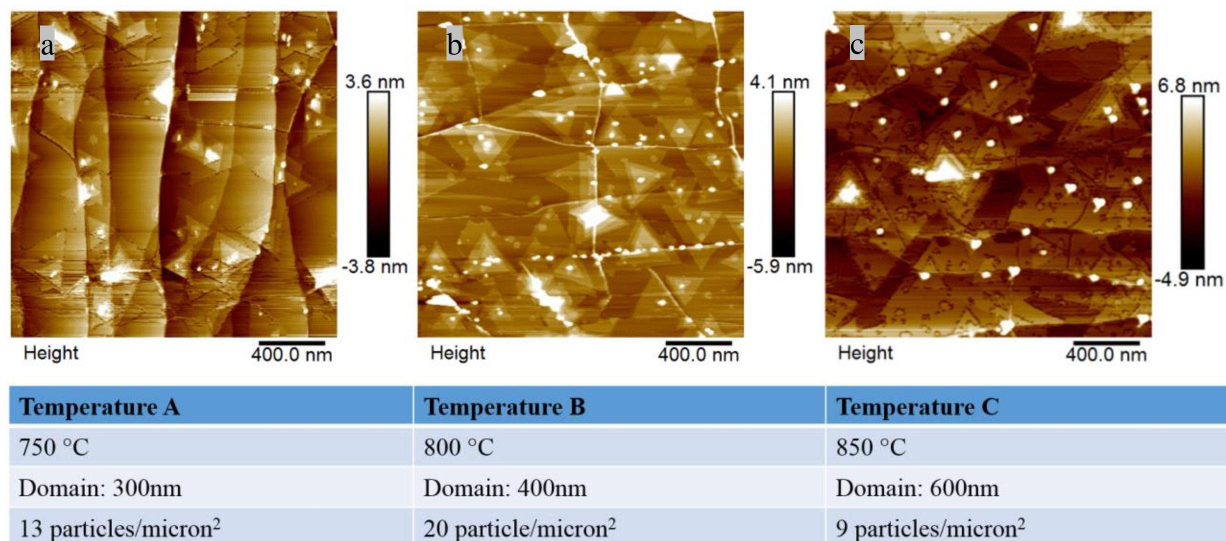

Temperature A	Temperature B	Temperature C
750 °C	800 °C	850 °C
Domain: 300nm	Domain: 400nm	Domain: 600nm
13 particles/micron^2	20 particle/micron^2	9 particles/micron^2

Figure 19. AFM images of epitaxial graphene grown at a Se:W ratio of 170 with varying temperature shows an increase in domain size as temperature increases. a) 750 °C; b) 800 °C; c) 850 °C

As seen in Figure 19, there was an increase in domain size from 300nm to 600nm as the growth temperature increased from 750 °C to 850 °C. There was no visible trend with the particle density of these samples, as the highest particle density of 20 particles/ square micron was found on the sample grown at 800 °C. When comparing the epitaxial graphene samples with sapphire samples grown simultaneously, the increased domain size and nucleation makes it evident that WSe_2 synthesizes on epitaxial graphene with more ease than on sapphire at lower Se:W ratios. Figure 20 shows the sapphire samples that directly correlate with the epitaxial graphene samples in Figure 19.

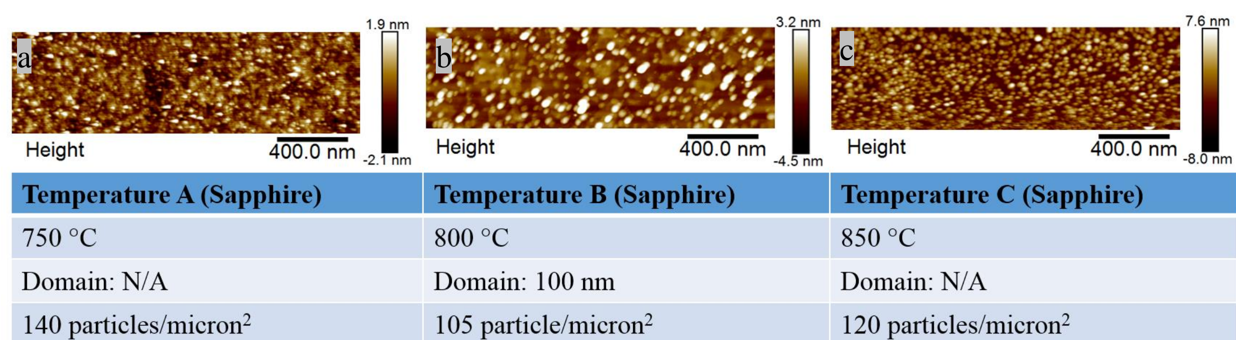

Temperature A (Sapphire)	Temperature B (Sapphire)	Temperature C (Sapphire)
750 °C	800 °C	850 °C
Domain: N/A	Domain: 100 nm	Domain: N/A
140 particles/micron^2	105 particle/micron^2	120 particles/micron^2

Figure 20. AFM images of WSe_2/sapphire samples grown at various growth temperatures show poor nucleation compared to the graphene in Figure 19.
a) 750 °C; b) 800 °C; c) 850 °C

Nucleation of WSe_2 triangles only appeared at 800 °C, and even the domain size of 100nm was low compared to the domain sizes of the equivalent epitaxial graphene sample, which was 400nm. A higher density of particulates formed on the sapphire compared to the epitaxial graphene, which correlates to the tungsten-rich particles for lower Se:W ratio trend on sapphire in Section 3.2.

Next, the effect of selenium to tungsten precursor ratio was analyzed. The ratios ranged from 170 to 700. Figure 21 shows FESEM images of these samples.

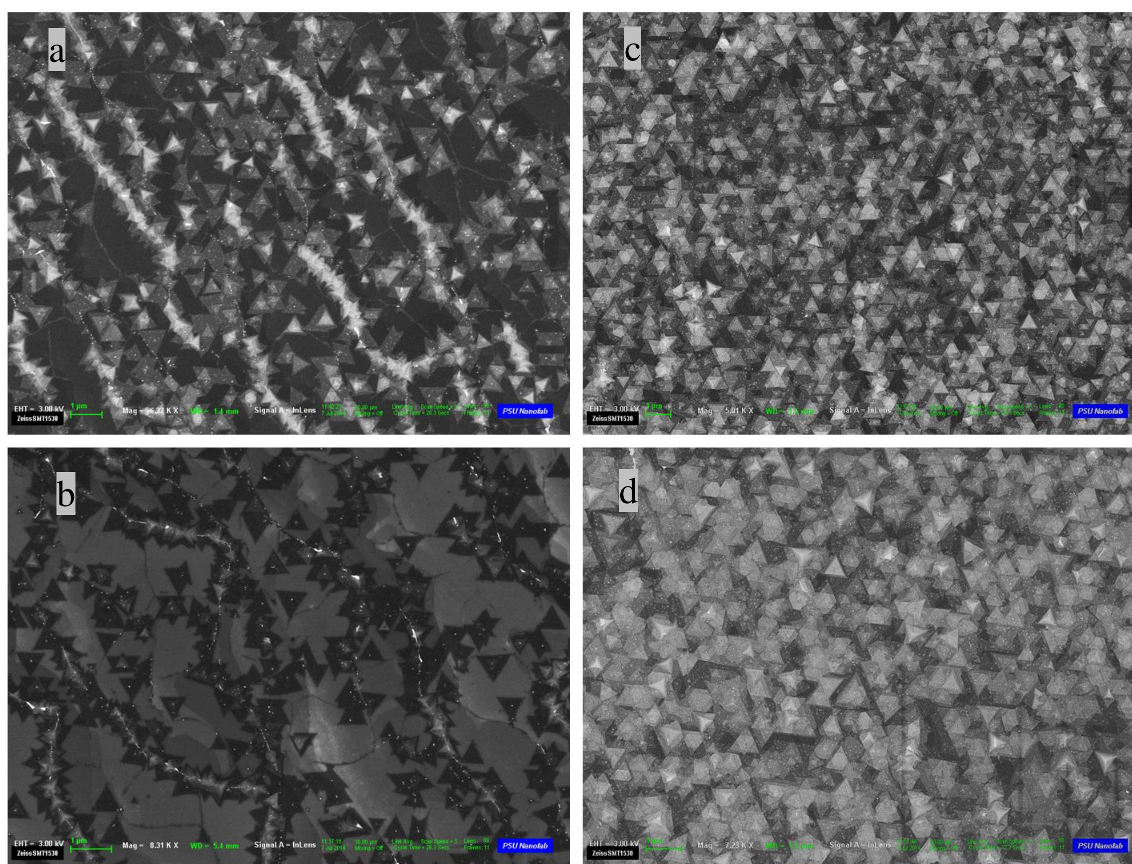

Figure 21. FESEM of WSe_2/EG samples demonstrate increased nucleation as Se:W increases. a) Se:W= 170 @ 825 ^oC; b) Se:W=500 @ 825 ^oC; c) Se:W=609 @ 800 ^oC; d) Se:W=700 @ 825 ^oC

The lower Se:W ratios demonstrates that nucleation sites form along the step edges of the epitaxial graphene, with the triangles orienting in the same direction. Additionally, bilayer triangles formed in the center of the monolayer triangles, signifying that secondary nucleation is from the center of pre-existing triangles. As the Se:W ratio increases, increased secondary nucleation occurs and monolayer triangles begin converging into a continuous film. Comparing the domain sizes for epitaxial graphene to sapphire at higher Se:W yields a shift in which substrate allows higher domain sizes. Figure 22 shows a comparison of a WSe_2/EG sample synthesized simultaneously with a WSe_2/Sapphire sample.

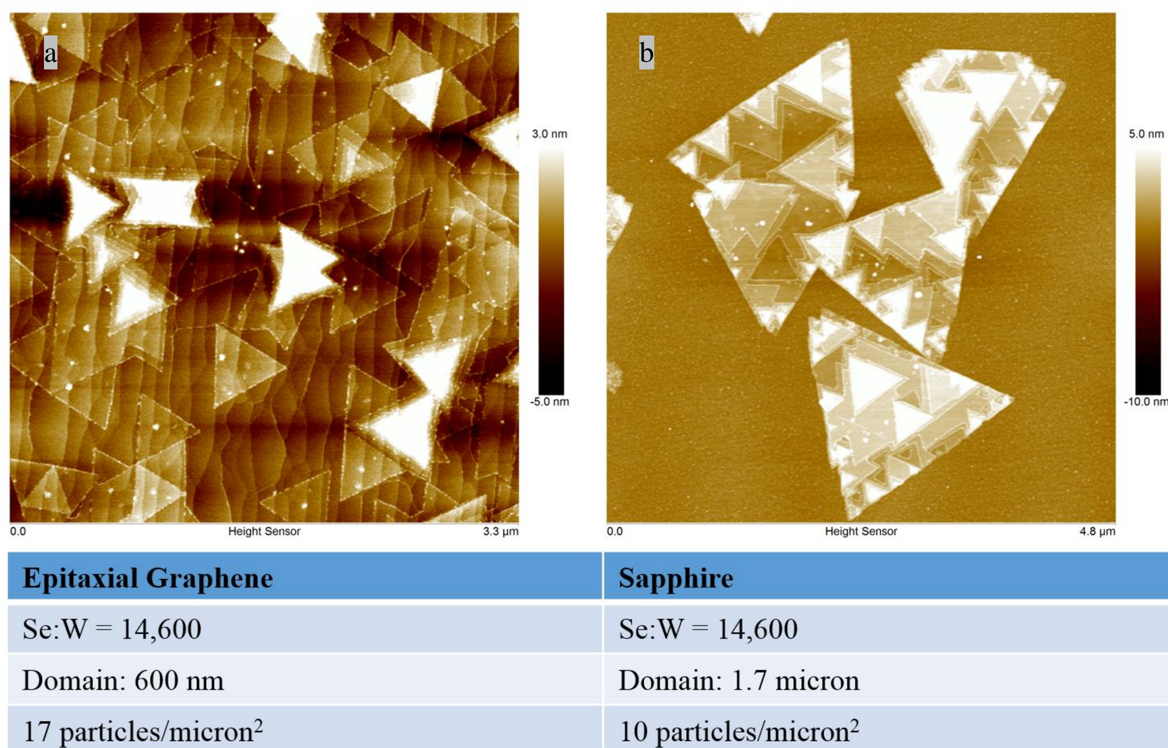

Epitaxial Graphene	Sapphire
Se:W = 14,600	Se:W = 14,600
Domain: 600 nm	Domain: 1.7 micron
17 particles/micron^2	10 particles/micron^2

Figure 22. AFM images of WSe_2/EG compared to WSe_2/Sapphire under same conditions at higher Se:W ratio. a) WSe_2/EG; b) WSe_2/Sapphire

The domain size on the sapphire sample of 1.7 microns was much larger than the 600nm domain size on the epitaxial graphene sample. Additionally, a lower particle density of 10 particles per square micron was observed on the sapphire compared to the 17 particles per square micron on the epitaxial graphene. Though the domain size was larger for the sapphire, the graphene exhibited more monolayer nucleation sites and greater coverage on the sample. This suggests that under optimal Se:W ratios, the sapphire yields larger WSe_2 triangles, although the nucleation sites of monolayer WSe_2 was greater for the graphene.

3.4 Tungsten Diselenide on Amorphous Boron Nitride

The third substrate analyzed was amorphous boron nitride. As stated in Section 1.3.4 on BN substrates, these samples were provided by AFRL pre-cleaned, so no additional cleaning was necessary. Similar to the studies on sapphire and epitaxial graphene, the effect of pressure was analyzed on boron nitride samples, as shown in Figure 23.

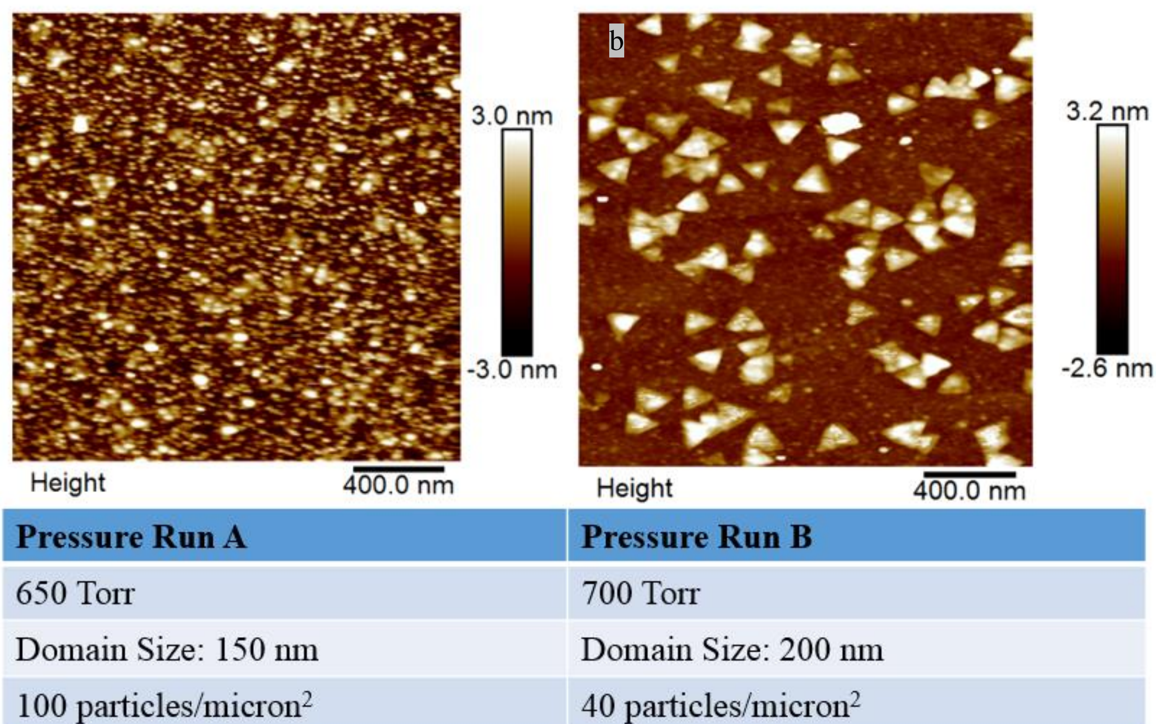

Pressure Run A	Pressure Run B
650 Torr	700 Torr
Domain Size: 150 nm	Domain Size: 200 nm
100 particles/micron^2	40 particles/micron^2

Figure 23. AFM of WSe_2/BN synthesized at different pressures show that increasing the pressure increases domain size and reduces particle density.
a) 650 Torr; b) 700 Torr

The sample in Figure 23a, which was grown at 650 Torr, exhibits heavy defect decoration, meaning the particle density for the 650 Torr (100 particles per square micron) was much higher compared to the 700 Torr sample in Figure 23b, which had only 40 particles per square micron. Next the effect of Se:W ratio was analyzed for the BN substrates, seen in Figure 24 below.

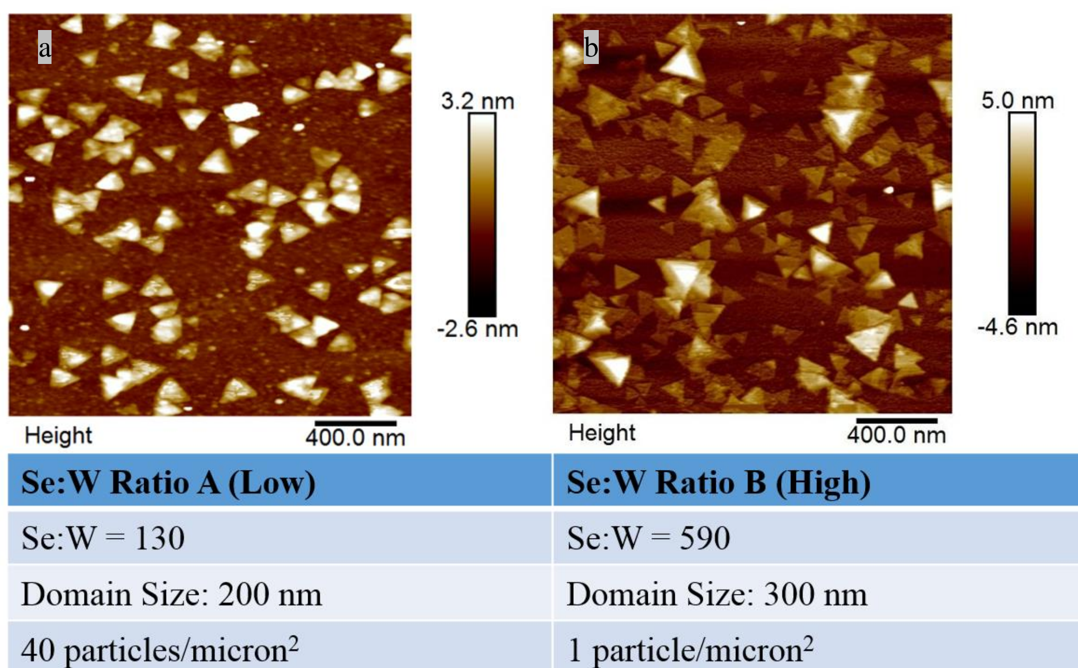

Se:W Ratio A (Low)	**Se:W Ratio B (High)**
Se:W = 130	Se:W = 590
Domain Size: 200 nm	Domain Size: 300 nm
40 particles/micron^2	1 particle/micron^2

Figure 24. AFM of WSe_2/BN at different Se:W ratios demonstrate an increased domain size with increased Se:W. a) Se:W=130; b) Se:W=590

Like the sapphire and epitaxial graphene substrates, amorphous boron nitride exhibited an increased WSe_2 domain size when the concentration of selenium precursor relative to the concentration of tungsten precursor was increased. Unlike the sapphire and epitaxial graphene substrates, however, the boron nitride exhibited limited WSe_2 lateral nucleation compared to the samples grown on sapphire substrates simultaneously. Figure 25 shows the AFM images of two sets of samples; the top two samples grown during the same run and the bottom two samples grown during another run. During each run, one sample was grown on sapphire substrate, and the other was grown on amorphous boron nitride.

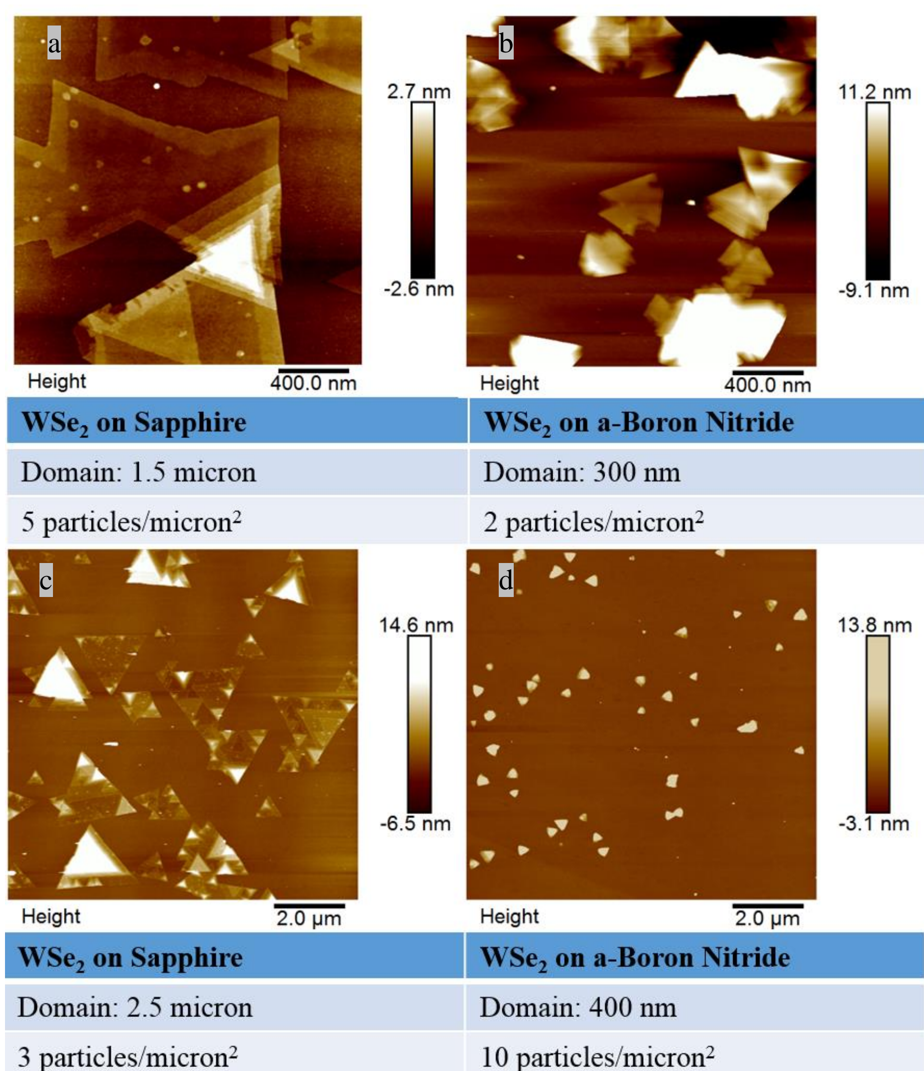

WSe_2 on Sapphire	WSe_2 on a-Boron Nitride
Domain: 1.5 micron	Domain: 300 nm
5 particles/micron^2	2 particles/micron^2

WSe_2 on Sapphire	WSe_2 on a-Boron Nitride
Domain: 2.5 micron	Domain: 400 nm
3 particles/micron^2	10 particles/micron^2

Figure 25. AFM images of WSe_2 on both a sapphire and amorphous boron nitride substrates synthesized under the same conditions. a) WSe_2/Sapphire with total H_2 flow = 100 sccm; b) WSe_2/a-BN with total H_2 flow = 100 sccm; c) WSe_2/Sapphire with total H_2 flow = 250 sccm; d) WSe_2/a-BN with total H_2 flow = 250 sccm

The boron nitride had more vertical nucleation than the sapphire, as seen in the height scale bar to the right of the top two AFM images. Also, the WSe_2 triangles only had a domain size of 300 nm and 400 nm on boron nitride, which is small compared to the 1.5 micron and 2.5 micron domain sizes of WSe_2 on the sapphire substrate.

Next, the total flow of hydrogen carrier gas through the MOCVD system during deposition was analyzed. Figure 26 shows the AFM comparison of two WSe_2/a-BN samples synthesized at 100 sccm of hydrogen and 250 sccm of hydrogen, respectively.

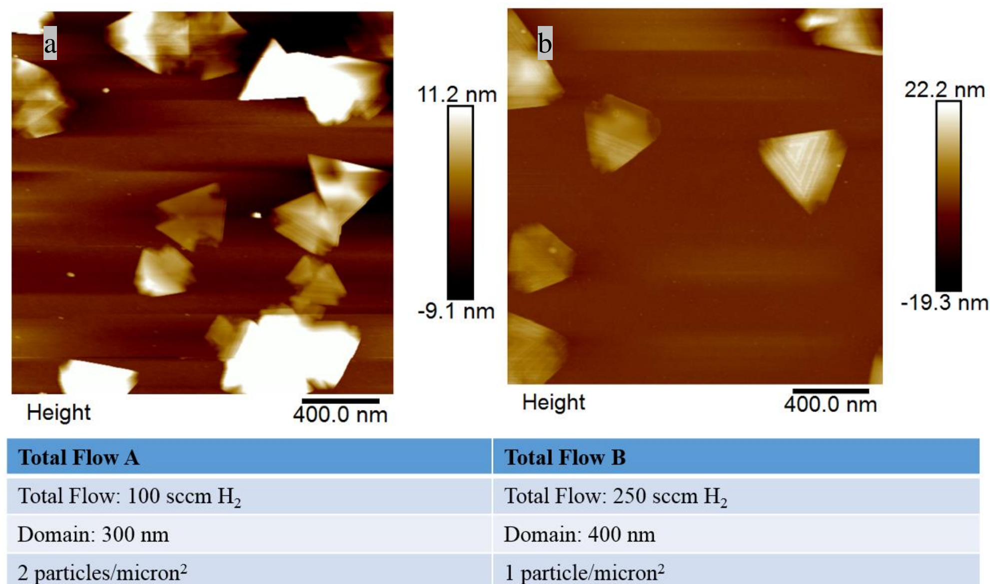

Total Flow A	Total Flow B
Total Flow: 100 sccm H_2	Total Flow: 250 sccm H_2
Domain: 300 nm	Domain: 400 nm
2 particles/micron^2	1 particle/micron^2

Figure 26. AFM images of WSe_2 on a-BN synthesized with different total flows of hydrogen in the MOCVD system. a) Total flow = 100 sccm H_2; b) Total flow = 250 sccm H_2

The AFM images confirm that higher flows of hydrogen in the MOCVD system during deposition allows more lateral nucleation to occur, seen in the increased domain size. This is due to the increased reaction rate at higher hydrogen flow rates. Also, the WSe_2/boron nitride sample grown at 250 sccm hydrogen exhibits a spiral-like pattern on the far-right triangle, signifying a screw dislocation growth mechanism in the formation of multilayers on the triangle. This suggests a different growth mechanism for growth on boron nitride compared to the layer-by-layer growth on sapphire substrates. Chen *et al.* observed screw dislocation of WSe_2 on SiO_2/Si substrates using their CVD growth method[11].

To try increasing the nucleation of tungsten diselenide on boron nitride surfaces an oxygen etch was conducted before growing the WSe_2. This etch would theoretically alter the

surface energy of the boron nitride to allow more lateral nucleation of WSe_2. Figure 27 shows the AFM of the amorphous boron nitride sample before and after the etching procedure.

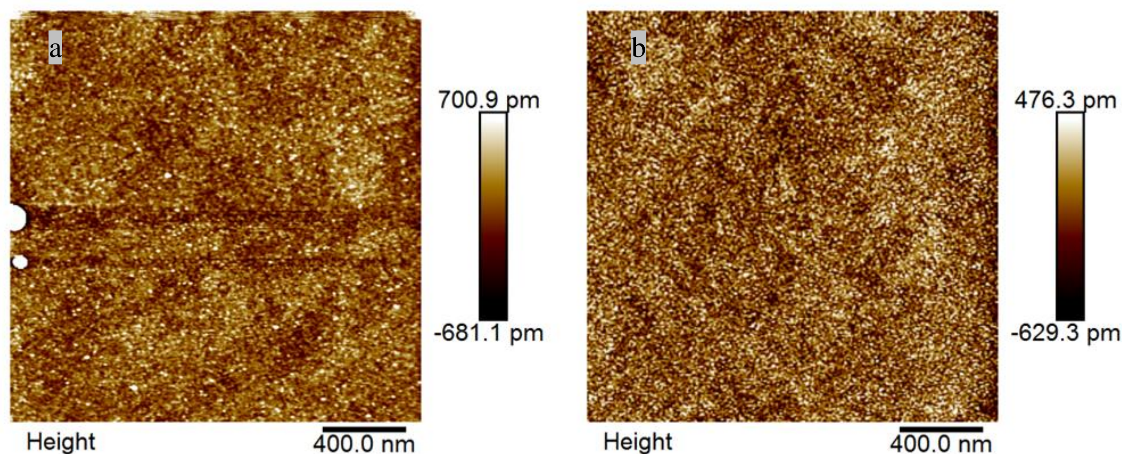

Figure 27. AFM of a-BN before and after an oxygen etch shows reduced roughness after etching. a) Pre-etched BN; b) Post-etched BN

Using the Nanoscope Analysis software, the average roughness (r_a) and the root mean square or RMS roughness (r_q) – which uses least squares calculations – were determined for both the pre-etched scan and the post-etched scan. Table 2 shows the respective roughness values.

Table 2. Roughness values for pre-etched BN compared to post-etched BN

	Pre-etched BN	**Post-etched BN**
Average Roughness (r_a)	0.148 nm	0.145 nm
RMS Roughness (r_q)	0.561 nm	0.183 nm

The values for both the average roughness and RMS roughness were higher for the pre-etched BN compared to the BN after etching, which suggests that etching the BN creates a smoother surface. Directly after the boron nitride sample was etched, the sample was placed in the MOCVD chamber, and tungsten diselenide was synthesized at a pressure of 700 Torr, a ratio of selenium to tungsten precursor of 10,200, a total flow of 250 sccm, an anneal at 500 °C for 15

minutes, a nucleation step at 700 °C for 2 minutes, and deposition at 900 °C for 30 minutes. The resulting film was analyzed under atomic force microscopy at several areas on the sample, shown in Figure 28.

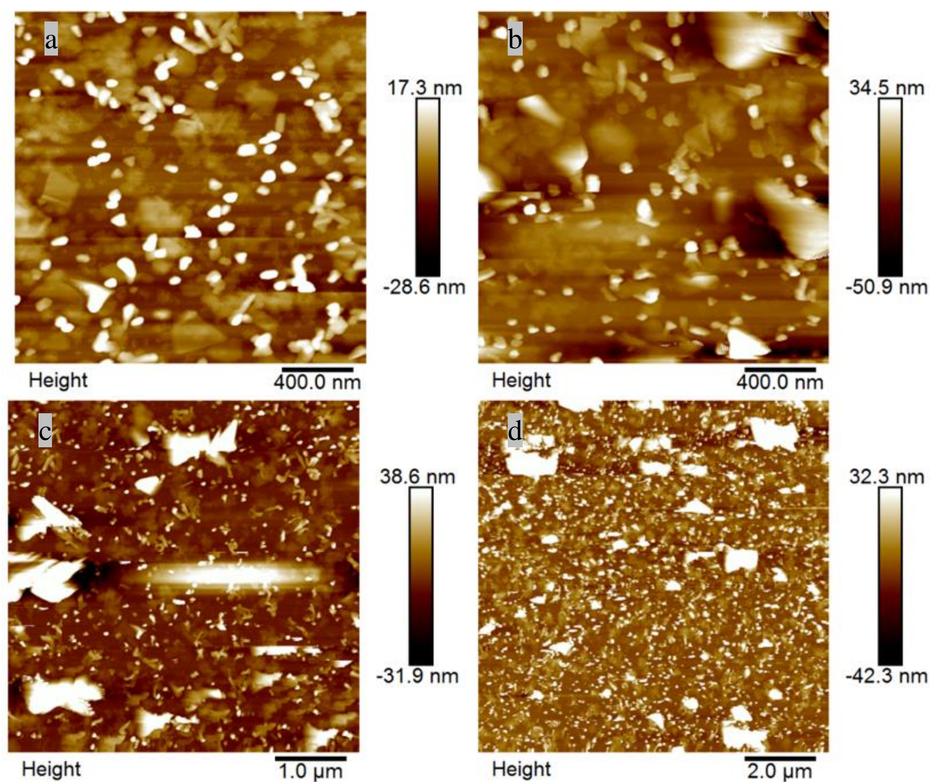

Figure 28. AFM of WSe_2 on etched a-BN shows high particle density of 25 particles/square micron and small domain size of 200nm. a-d) different areas on the sample

The WSe_2 on etched boron nitride exhibited high particle density with 25 particles per square micron. This nucleation density was higher than the nucleation density on the previous boron nitride samples. Additionally, the average domain size of the WSe_2 triangles was 200nm with a standard deviation of +/- 45 nm, which was low compared to the other boron nitride samples analyzed.

CHAPTER 4

CONCLUSION

As taught in the Materials Science and Engineering classes at The Pennsylvania State University, there is a direct correlation between the process of synthesizing a material and the material's resulting properties. Included in this report are an explanation of the techniques used to synthesis tungsten diselenide thin films and the motivation for choosing metal organic chemical vapor deposition, a description of the experimental setup with a focus on the parameters for deposition onto different substrates; as well as a discussion of the results in the experimentation. The purpose of this thesis is to provide an analysis of the impact of several parameters on the synthesis of tungsten diselenide, such as substrate, temperature, pressure, precursor concentrations, and growth time.

Results showed that increasing the growth pressure from 600 Torr to 700 Torr increased the nucleation of tungsten diselenide triangles, as did increasing the growth temperature from 700 °C to 900 °C. The disadvantage of higher temperatures and pressures was the increase in particulates on the surface. Analyzing the effect of selenium to tungsten concentration ratios, the higher particle density with lower Se:W ratio determined that deficient amounts of selenium left tungsten-rich particles on the surface. Increasing the selenium concentration relative to the tungsten precursor did in fact increase the domain size of tungsten diselenide and reduce particulates. There was a limit to the ratio, for after a Se:W ratio of 100,000 the domain size dropped back down and particle density increased.

The substrates exhibited varying levels of ease with forming large lateral growth of tungsten diselenide. The epitaxial graphene exhibited the biggest domain sizes under similar conditions, and WSe_2 triangles formed along the step edges of the graphene. Sapphire substrates

exhibited a layer-by-layer growth mechanism, seen in the stacking of multilayer triangles above the monolayer triangles, and the growth process was optimized to produce up to 8 micron triangles. Because domain sizes of WSe_2 were smallest for the amorphous boron nitride substrates compared to sapphire and epitaxial graphene, BN exhibited the most resistance to lateral nucleation of tungsten diselenide compared to the other substrates, and the growth mechanism, a screw dislocation, was different than the other substrates. Future work of optimizing the deposition parameters for better WSe_2 nucleation on boron nitride could see scalable synthesis for future optical and electronic materials.

BIBLIOGRAPHY

[1] W. Zhao, Z. Ghorannevis, L. *et al*. Evolution of electronic structure in atomically thin sheets of WS_2 and WSe_2. *ACS Nano*. **2012**, *7*, 791–797.

[2] Yan, T., Qiao, X., *et al.* Photoluminescence properties and exciton dynamics in monolayer WSe_2. *Appl. Phys. Lett.* **2014**, *105*, 101901

[3] Galen, E., Cohen, H., *et al.* Crystallization of layered metal-dichalcogenides films on amorphous substrates. *Appl. Phys. Lett.*, **1995**, *67* (23).

[4] Salitra, G., Hodes, G., Klein, E., Tenne, R. Highly oriented WSe_2 thin films prepared by selenization of evaporated WO_3. *Thin Solid Films*. **1994**, *245*, 180.

[5] Schmidt, P., Binnewies, M. Chemical Vapor Transport Reactions – Methods, Materials, Modeling. *InTech.* **2013**, *10*.5772, 55547.

[6] Patel, PR, Patel, KR, Pathak, VM. Growth and Characterization of WSe_2 Single Crystals. *J. Adv. Dev. Res.* **2012**, *Vol. 3*, No. 1.

[7] Clark, G., Wu, S., Rivera, P., *et al.* Vapor-transport growth of high optical quality WSe_2 monolayers. *APL Materials*. **2014**, *2*, 101101.

[8] Cheung, N. Chemical Vapor Deposition. Presented at University of California Berkeley, Berkeley, CA, 2010.

[9] Shi, Y., Li, H., Li, *et al.* Recent advances in controlled synthesis of two-dimensional transition metal dichalcogenides via vapour deposition techniques. *Chem. Soc. Rev.* **2015**, *44*, 2744-2756.Nguyen, B., Than, X., *et al.* Fabrication of horizontally aligned ultra-long single-walled carbon nanotubes on Si substrates using the fast-heating chemical vapor deposition method. *Adv. Nat. Sci: Nanosci. Nanotechnol.* **2012**, *3*, 025010.

[10] Huang, J.K., Pu, J., *et al*. Large-Area and Highly Crystalline WSe_2 Monolayers: from Synthesis to Device Applications. *ACS Nano*. **2014**¸ *8*(1), 923-930.

[11] Chen, L., Liu, B., Abbas, A., *et al*. Screw-Dislocation-Driven Growth of Two-Dimensional Few-Layer and Pyramid-Like WSe_2 by Sulfur-Assisted Chemical Vapor Deposition. *ACS Nano*. **2014**, *8* (11): 11543-51.

[12] Tutorial 3 – MOCVD: Bubblers. *Precisionfab.net.* Precision Fabricators Ltd. Website.

[13] Eichfeld, S., Hossain, L., *et al.* Highly Scalable, Atomically Thin WSe_2 Grown via Metal-Organic Chemical Vapor Deposition. *ACS Nano*, **2015**, *Vol. 9*, 2080-2087.

[14] Lai, K., Lamb, H. Tungsten chemical vapor deposition using tungsten hexacarbonyl: microstructure of as-deposited and annealed films. *Thin Solid Films*. **2000**, *370*, 114-121.

[15] Mishra, S., Jeanneau, E., Daniele, S. Dimethyl selenide complexes of copper, gallium and indium halides as potential precursors for selenium-containing chalcopyrite semiconducting materials. *Polyhedron*, **2010**, *29*, 500-506.

[16] Perevalov, T.V., Tereshenko, O. E., *et al*. Oxygen deficiency defects in amorphous Al_2O_3. *Journal of Applied Physics*. **2010**, *108*, 013501.

[17] Sapphire (Al_2O_3). MolTech GmbH, **2013.** http://www.mt-berlin.com/frames_cryst/ descriptions/sapphire.htm. Web.

[18] Lin, Y., Chang, C., *et al*. Atomically Thin Heterostructures Based on Single-Layer Tungsten Diselenide and Graphene. *Nano Lett.* **2014**, *14*, 6936-6941.

[19] Pakdel, A., Bando, Y., Golberg, D. Nano boron nitride flatland. *Chem So. Rev.,* **2014**, *43*, 934.

[20] Paine, R., Narula, C. Synthetic Routes to Boron Nitride. *Chemical Reviews***, 1990,** *Vol. 90*, No. 1.

[21] K. Novoselov, D. Jiang, F. Schedin, T. Booth, V. Khotkevich, S. Morozov, and A. Geim, "Two-dimensional atomic crystals," *Proc. Natl. Acad. Sci. U. S. A*. **2005,** *102*, 10451–10453.

[22] Terrones, H., Del Corro, E., *et al*. New First Order Raman-Active Modes in Few Layered Transition Metal Dichalcogenides. *Sci. Rep*. **2014**, *4*, 4215.

[23] Gfroerer, T. Photoluminescence in Analysis of Surfaces and Interfaces. Encyclopedia of Analytical Chemistry. Meyers, R.A. (Ed.). *John Wiley & Sons Ltd.*, **2000**. pp. 9209-9231

[24] Information on the FESEM (Field-emission Scanning Electron Microscope). *http://www.vcbio.science.ru.nl/* Radboud University Nijmegen: Virtual Classroom Biology. Web.

303 Hillcrest Drive
Edinboro, PA 16412

lah5413@psu.edu
(814) 464-6047

ACADEMIC VITA

Lorraine Hossain

Objective — Graduate research program as a Materials Science and Engineer

Education

Bachelor of Science, Materials Science and Engineering — August 2011-Present
Nanotechnology minor — Schreyer Honors College Scholar
The Pennsylvania State University: University Park

Research Experience

08/2012 – Present — **Researcher, Center for 2D and Layered Materials at Penn State**

- 2D Materials Lab with Dr. Joshua Robinson (Asst. Director, 2DLM)
- Researched synthesis of electronic materials (WO_3,WSe_2) via CVT & CVD

05/2013 – 08/2013 — **Research Fellow, Penn State Summer Discovery Grant**

- Researched chemical vapor transport synthesis of WSe_2 from WO_3 and Se

01/2012 – 06/2012 — **Women in Science and Engineering Researcher, Penn State**

- Pennsylvania Space Grant's 2012 Undergraduate Research program
- Phases Research Lab; Dr. Zi-Kui Liu (Director, Center for Comp. Materials Design)
- Researched MgZn diffusion couples and phase stability

Academic Experience

Global Renewable Energy Education Network (GREEN)-Costa Rica Program Alumna
Reykjavik University with GREEN-Iceland Sustainability Program Alumna
SRCC, University of Delhi and IIS University with SHC - Indo-US Exchange Alumna
The GLOBE Scholar Assistant through the Schreyer Honors College

Leadership Experience

Learning Assistant, Honors Chemistry at Penn State, 2014
Senior Class Representative, Material Advantage, 2014-2015
Cultural Secretary/Undergrad Representative, Bangladeshi Student Assoc., 2013-2015
Active member, Keramos (Ceramic Engineering Honorary Fraternity), 2012-2015
Active member, Society of Women Engineers, TMS, ASM, AIST, ACerS, 2011-2015
Volunteer, Thrifty Threads, 2009-2015
President, Material Advantage, 2013-2014
President, PSU Natya, 2012-2014
Instructor, Bharatanatyam classical Indian dance, 2007-2011
Valedictorian with GPA: 4.50/4.00, General McLane High School, 2011

Skills

Trained on Raman, AFM, FESEM, CVD/CVT furnaces, Plasma-Therm Dep.
Familiar with MATLAB, Materials Studio, VMD, Crystal Maker

Achievements

Dean's List Fall 2011, Spring 2012, Fall 2013, Spring 2014, Fall 2014
2014 David W. Richerson Service Award in Materials Science
ND-Connect 2013 research initiation prize recipient
Schreyer Honors Academic Excellence Scholarship
E. Wayne Kay Undergraduate Scholarship (Society of Manufacturing Engineers)

Publications

Eichfeld, S.; Hossain, L.; Lin, Y.; Robinson, J.; *et al*. (2015) Highly Scalable, Atomically Thin WSe2 grown via Metal-Organic Chemical Vapor Deposition. ACS Nano. nn5073286.

Eichfeld, S., Eichfeld, C., Lin, Y., Hossain, L., Robinson, J., (2014). Rapid, non-destructive evaluation of ultrathin WSe_2 using spectroscopic ellipsometry. APL Materials 2, 092508.

Azizi, A.; Eichfeld, S.; Geschwind, G.; Hossain, L.; *et al*. (2015) Freestanding van der Waals Heterostructures. Adv. Matl. adma.201404938. (pending)

Browning, P.; Eichfeld, S.; Zhang, K.; Hossain, L.; *et al*. (2015) Large-area synthesis of WSe_2 from WO_3 by selenium-oxygen ion exchange. 2D Materials. 2, 014003.